AGU PUBLICATIONS

JGR

Journal of Geophysical Research: Atmospheres

RESEARCH ARTICLE
10.1002/2015JD023404

Key Points:
- The LSM spin-up time depends on the complexity of the model physics
- Adding impacts from the mucilage in the rhizosphere produces better results
- Uncertainties in soil initialization and forcing conditions are discussed

Correspondence to:
Y. Gao,
gaoyh@lzb.ac.cn

Citation:
Gao, Y., K. Li, F. Chen, Y. Jiang, and C. Lu (2015), Assessing and improving Noah-MP land model simulations for the central Tibetan Plateau, *J. Geophys. Res. Atmos.*, *120*, 9258–9278, doi:10.1002/2015JD023404.

Received 22 MAR 2015
Accepted 21 JUL 2015
Accepted article online 25 JUL 2015
Published online 23 SEP 2015

Assessing and improving Noah-MP land model simulations for the central Tibetan Plateau

Yanhong Gao[1], Kai Li[1], Fei Chen[2,3], Yingsha Jiang[1], and Chungu Lu[4]

[1]Key Laboratory of Land Surface Process and Climate Change in Cold and Arid Regions, Cold and Arid Regions Environmental and Engineering Research Institute, Chinese Academy of Sciences, Lanzhou, China, [2]National Center for Atmospheric Research, Boulder, Colorado, USA, [3]State Key Laboratory of Severe Weather, Chinese Academy of Meteorological Sciences, China Meteorological Administration, Beijing, China, [4]National Science Foundation, Arlington, Virginia, USA

Abstract The Tibetan Plateau (TP) region experiences strong land-atmosphere interactions, and as an elevated heating source, significantly influences the formation of the Asian monsoon. Those interactions are not well represented in current land-surface models (LSMs), partly due to difficulties in representing heterogeneities in soil structures in LSM. Simulations using the Noah with multiparameterization options (Noah-MP) LSM are employed to assess the relative importance of parameterizing vertical soil heterogeneity, organic matter, and soil rhizosphere and their impacts on seasonal evolution of soil temperature, soil moisture, and surface energy and water budgets at the sparsely vegetated Amdo site located in central TP. The LSM spin-up time at the central TP depends on the complexity of the model physics, ranging from 4 years with simplest soil physics to 30 years with the addition of organic matter and spare to dense rhizosphere parameterization in Noah-MP. Representing layered soil texture and organic matter does not improve low biases in topsoil moisture. Reducing the saturated conductivity from the mucilage in the rhizosphere produces better results. Surface sensible and latent heat fluxes are better simulated in the monsoon season as well. Adding layered soil texture and organic matter in Noah-MP retard the thawing in deep soil layers, and the rhizosphere effect delays thawing even more in the transient season. Uncertainties in soil initialization significantly affect deep-soil temperature and moisture, but uncertainties in atmospheric forcing conditions mainly affect topsoil variables and consequently the surface energy fluxes. Differing land-surface physics cause 36% uncertainty in the accumulated evapotranspiration and subsurface runoff.

1. Introduction

Understanding of the interactions between land surfaces and the atmosphere helps improve numerical weather prediction [*Chen et al.*, 2001; *Chen and Zhang*, 2009; *Chang et al.*, 2009; *Trier et al.*, 2004, 2008; *Kumar et al.*, 2014; *Barlage et al.*, 2015; *Rasmussen et al.*, 2011]. In these interactions, terrestrial water budgets control the dryness/wetness of a given region. The evapotranspiration provides water vapor from the land surface to the overlay atmosphere and affects stability of the planetary boundary layers and precipitation initiation [*Trier et al.*, 2004, 2011; *Gao et al.*, 2008; *Xue et al.*, 2012; *LeMone et al.*, 2013, 2014]. However, the regional evapotranspiration could not be measured with the same quality as precipitation, and it is usually estimated using a land-surface model (LSM) and remote sensing [*Bolten et al.*, 2004; *Lakshmi*, 2004]. Several generations of LSMs have been developed in recent decades for their use in weather and climate models [*Dickinson et al.*, 1986; *Sellers et al.*, 1996; *Chen and Dudhia*, 2001; *Dai et al.*, 2003; *Niu et al.*, 2011]. Despite continuous improvements in LSMs regarding their capability of simulating surface heat fluxes and hydrologic components, discrepancies still remain, particularly in areas with high degrees of surface heterogeneity and sparse vegetation [*Zhang et al.*, 2014a, 2014b].

The Tibetan Plateau (TP) is a region that experiences strong land-atmosphere interactions. It has been widely accepted that the TP provides an elevated heating source to the middle troposphere, and therefore, the land-atmosphere interactions play an important role in the formation of the Asian monsoon [*Yeh and Gao*, 1979; *Yanai et al.*, 1992; *Yanai and Wu*, 2006; *Xu et al.*, 2010]. However, land-atmosphere interactions over the TP are not well represented in current LSMs coupled to weather and climate models [*Yang et al.*, 2005; *Yang et al.*, 2009; *Chen et al.*, 2012]. For instance, studies found significant underestimation of the LSM-simulated soil liquid water (SLW) content in the topsoil in the central TP [*Yang et al.*, 2005]. Among efforts to mitigate this discrepancy, *Yang et al.* [2005] indicated that the vertically heterogeneous soils affect soil subsurface processes and play an important role in controlling surface-soil wetness and surface energy partition. Also, the soil organic

Figure 1. Landscape conditions over the central TP.

matter within the topsoil is important in changing the profile of soil moisture in the central and eastern TP besides the soil stratification beneath the alpine meadows [*Yang et al.*, 2009]. Recently, *Chen et al.* [2012] investigated the stratification of soil thermal properties induced by soil organic carbon and its impact on the parameterization of the thermal properties. They attributed the underestimation in the topsoil to the soil organic carbon-caused stratification. Those studies focused on the soil stratification due to either soil texture heterogeneity or soil organic matter.

Similarly, vegetation has strong interactions with land-atmosphere energy and moisture fluxed [*Matsui et al.*, 2005]. The soil near vegetation roots is called the rhizosphere [*Darrah*, 1993; *Hinsinger et al.*, 2005; *Gregory*, 2006]. Heavily influenced by vegetation roots and microorganism activities, the rhizosphere develops different biological, chemical, and physical properties from those of the bulk soil [*Darrah*, 1993; *Hinsinger et al.*, 2005; *Gregory*, 2006; *Carminati et al.*, 2010; *Moradi et al.*, 2011; *Hinsinger et al.*, 2009]. As for physical properties, especially hydraulic properties (soil water retention curve and hydraulic conductivity), they may be affected by polymeric substances such as mucilage released by roots [*Moradi et al.*, 2011; *Nakanishi et al.*, 2005]. Due to its viscosity, mucilage is believed to clog pores and significantly decrease the soil-saturated conductivity [*Carminati et al.*, 2011; *Or et al.*, 2007] leading to a higher water-holding capacity for the rhizosphere [*Chenu*, 1993; *McCully and Boyer*, 1997; *Moradi et al.*, 2011; *Read et al.*, 1999; *Roberson and Firestone*, 1992; *Watt et al.*, 1994]. Similar effects of rhizosphere on soil hydraulic properties are discussed in subsequent observations [*McCully and Boyer*, 1997; *Nakanishi et al.*, 2005; *Carminati et al.*, 2010; *Reeder et al.*, 2014]. *Yen* [2001] indicated that the decreased degree of soil-saturated conductivity could reach 4 orders of magnitude. *Reeder et al.* [2014] found 3 orders reduction of the soil-saturated conductivity through the laboratory experiments. The vegetation is sparse in the central TP due to the cold and arid climate, and consequently, the vegetation roots are usually located in shallow soils (Figure 1). There is no in situ or laboratory measurement of root impact conducted over the TP. It is necessary to explore the shallow root impacts over there through the sensitive tests to provide guidance for the undergoing Third Tibetan Experiments [*Li et al.*, 2015].

The Noah LSM with multiparameterization options (Noah-MP) is a new-generation, community model and widely used in the research and operational communities [*Niu et al.*, 2011; *Yang et al.*, 2011; *Barlage et al.*, 2015]. While there exist focused efforts to validate the Noah-MP LSM for various land-cover types [*Niu et al.*, 2011; *Chen et al.*, 2014; *Cai et al.*, 2014], little is known about its applicability to the TP region. Therefore, the main goal of this study is to assess the relative importance of representing different soil processes (vertical soil heterogeneity, organic matter, and soil rhizosphere) in Noah-MP and specifically to investigate the impacts of the above parameterizations on the seasonal evolution of soil temperature, soil moisture, and surface energy and water budgets at the Amdo site located in central TP. Effects of uncertainties in the model physics, initialization, and atmospheric forcings on the simulated soil temperature and moisture for this site are discussed. Such a study is useful to provide guidance to improving the Noah-MP model and hence the Weather Research and Forecasting (WRF)-simulated land-atmosphere interactions over the TP region. The paper is organized as follows: section 2 describes the Noah-MP model, configuration, and data used. Section 3 discusses the LSM spin-up and analyzes results from various Noah-MP experiments. The summary is presented in section 4.

2. Description of the Noah-MP Model and Data Used

2.1. The Noah-MP Land-Surface Model

Noah-MP is a new-generation of LSM, based on the Noah LSM [*Chen et al.*, 1996; *Chen and Dudhia*, 2001], which is coupled to the WRF community weather and regional climate models [*Barlage et al.*, 2015]. It provides a unique multiparameterization framework that allows running the model with different combinations

Table 1. Noah-MP Parameterization Options Used in This Study

Parameterizations Description	Schemes Used
Dynamic vegetation	4: table LAI, shdfac = maximum
Stomatal resistance	1:Ball-berry, related to photosynthesis [*Ball et al*., 1987]
Soil moisture factor controlling stomatalResistance	1:Noah scheme, function of moisture [*Chen and Dudhia*, 2001]
Runoff and groundwater	2: SIMTOP [*Niu et al*., 2005]
Surface exchange coefficient for heat	1: M-O [*Brutsaert*, 1982]
Supercooled liquid water in frozen soil	2: Koren99 [*Koren et al*., 1999]
Frozen soil permeability	1:NY06 [*Niu and Yang*, 2006]
Radiation transfer	3: gap = 1—FVEG
Snow surface albedo	2: CLASS [*Verseghy*, 1991]
Partitioning precipitation into rainfall and snowfall	1: Jordan91 [*Jordan*, 1991]
Lower boundary condition of soil temperature	1: zero flux
The first-layer snow or soil temperature time scheme	1: semiimplicit

of alternative process schemes for individual land processes [*Niu et al*., 2011]. Noah-MP simulates several biophysical and hydrological processes that control surface fluxes between the surface and the atmosphere. These processes include surface exchange coefficients for heat, radiation interactions with the vegetation canopy and the soil, as well as the hydrological processes within the canopy and the soil, a multilayer snowpack, frozen ground, an unconfined aquifer model for groundwater dynamics, stomatal conductance, and photosynthesis. We used Noah-MP v1.1 in an off-line stand-alone 1-D mode with atmospheric forcing at a temporal resolution of 30 min. The atmospheric forcing includes downward shortwave and longwave radiation, wind speed, temperature, precipitation, relative humidity, and surface air pressure. The Noah-MP physics options used in our study are similar to *Barlage et al*. [2015] and *Chen et al*. [2014] and are listed in Table 1. In the default configuration of Noah-MP, soil texture and corresponding parameters are assumed to be unique in the entire soil column, and no soil organic matter or rhizosphere is included.

To evaluate effects of soil processes, we modified Noah-MP to include

1. Vertical heterogeneity in soil layers. Soil hydraulic parameters and thermal parameters are set to be an array of soil layers as function of soil texture [*Cosby et al*., 1984; *Peters-Lidard et al*., 1998]. The soil hydraulic parameters include the porosity, saturate hydraulic conductivity, *b*-curve slope, hydraulic potential, field capacity, wilt point, and saturated soil water diffusivity. Soil thermal parameters include the dry thermal conductivity, saturated thermal conductivity, and thermal capacity. *Yang et al*. [2005] documented an observed soil texture at 5 cm, 20 cm, and 60 cm depths at the Amdo site, which are used as the soil texture at upper three layers in Noah-MP, and the fourth layer uses the same texture at 60 cm depth. The soil hydraulic and thermal parameters at each layer are calculated using equations in *Cosby et al*. [1984] and *Chen and Dudhia* [2001].
2. Organic matter parameterization. The soil parameters are changed to be $A_i = (1 - V_{\mathrm{soc},i})A_{m,i} + V_{\mathrm{soc},i}A_{soc}$, in which i is the layer, A_i is the parameter, and A_{soc} are the hydraulic and thermal parameters of the organic matter. Soil porosity, saturated hydraulic conductivity, water potential, and *b*-curve slope are defined as $0.9\,\mathrm{m}^3\,\mathrm{m}^{-3}$, $1.0\times10^{-4}\,\mathrm{ms}^{-1}$, 10.3 mm, and 2.7, respectively, according to *Lawrence and Slater* [2008]. $V_{\mathrm{soc},i}$ is the volume percentage of the organic matter and calculated as

$$V_{\mathrm{soc},\ i} = \frac{\rho_p\left(1-\theta_{\mathrm{sat},m,i}\right)\mathrm{m}_{\mathrm{soc},i}}{\left[\rho_{\mathrm{soc}}\left(1-\mathrm{m}_{\mathrm{soc},i}\right)+\rho_p\left(1-\theta_{\mathrm{sat},m,i}\right)\mathrm{m}_{\mathrm{soc},m,i}+\left(1-\theta_{\mathrm{sat},m,i}\right)\frac{\rho_{\mathrm{soc}}\mathrm{m}_{g,i}}{\left(1-\mathrm{m}_{g,i}\right)}\right]},$$

where ρ_p is the density of the mineral soil, ρ_{soc} is the bulk density of the organic matter, $\theta_{\mathrm{sat},m}$ is the porosity of the organic matter, and $m_{\mathrm{soc},i}$ and $m_{g,i}$ are the organic and gravel percentages at each layer. Soil texture and soil organic matter measurements in *Yang et al*. [2005] and *Chen et al*. [2012] are used (Table 2) in this study.

Rhizosphere: vegetation roots are rather shallow at Amdo site compared with the flatland due to the cold and arid climatology in the TP. Therefore, only the rhizosphere impact is considered in the first soil layer. According to *Or et al*. [2007], the rhizosphere water-holding capacity is thousands of times smaller than that of the bulk soil. Therefore, for sensitivity tests, the saturated conductivity of the 0.1 m topsoil is set to be 10^{-1}–10^{-3} times smaller of the normal soil, respectively.

Table 2. Vertical Soil Texture and Organic Matters in Simulations (From *Yang et al.* [2005] and *Chen et al.* [2012]) for the Control (CTL), Soil Vertical Stratification (LAY), and Soil Organic Matter (SOM)

	Layer	SOC %	Sand %	Clay %	Gravel %	Soil Type
CTL	1–4	-	72	8		sand loam
LAY	1	-	30.64	9.48		silt loam
	2	-	70.86	8.65	3.92	sand loam
	3	-	79.21	10.32	3.35	sand loam
	4	-	79.21	10.32		sand loam
SOM	1	3.1		The same as Exp2		silt loam
	2	1.13				sand loam
	3	0				sand loam
	4	0				sand loam

2.2. Observation Sites and Soil/Vegetation Parameters

This study focuses on the Global Energy and Water Cycle Experiment Asian Monsoon Experiment on the Tibetan Plateau (GAME/Tibet, 1996–2000) intensive observing period (16 May to 26 September 1998) conducted in the central TP (http://wdcdgg.westgis.ac.cn/chinese/DATABASE/Game_Tibet/plateau98.jpg). The Anduo (also named Amdo in GAME/Tibet, elevation ~4700 m) was selected for this study, because it is located in an alpine meadow—a typical and dominant vegetation type in the central TP and collected a more comprehensive array of measurements. Under the influence of winter westerlies, the local climate at Amdo is cold and dry with a long frozen-ground season from October to June. During the summer, it is typically affected by the Asian monsoon. The amount of precipitation is only 7 mm during the premonsoon season but reaches 278 mm during the monsoon season [*Yang et al.*, 2005, 2009]. The onset of the plateau monsoon in 1998 was 15 June, which was later than that in normal monsoon years [*Yang et al.*, 2005]. The land surfaces are characterized by nearly bare soils in the premonsoon season but turn to grassland afterward. The vegetation is sparse in the central TP due to the cold and arid climate, and consequently, the vegetation roots grow in shallow soils (Figure 1).

During 16 May to 26 September 1998, site measurements included precipitation, radiation, soil moisture, and turbulent fluxes. SLW was measured by the time domain reflectometer and turbulence fluxes by eddy-covariance system. Data averaged over each interval of 30 or 60 min were recorded. The surface temperature was converted from downward and upward longwave radiation with the surface emissivity derived from observations [*Yang et al.*, 2008]. Missing data from 6 to 15 June were gap filled using the nearby flux-tower observations. The net surface radiation and ground heat flux are observed. Several independent studies have demonstrated that the observed latent and sensible fluxes are prone to severe errors at this site [*Tanaka et al.*, 2003; *Yang et al.*, 2004; *Su et al.*, 2006]. Alternatively, the sensible and latent heat fluxes are calculated based on the observations using the Bowen ratio approach. This approach has been used in prior studies and proved agreeing well with results from other approaches well [*Yang et al.*, 2009]. The vegetation type is set to grassland according to *Yang et al.* [2005], and the monthly 10 year climatology SPOT/VEG leaf area index (LAI) at Amdo is used [*Baret et al.*, 2013]. Monthly LAI are 0.23, 0.51, 0.92, 0.92, and 0.62 from May to September, respectively.

2.3. Forcing Data

LSM spin-up is necessary to obtain equilibrium soil states, which would require long-term forcing conditions [*Chen and Mitchell*, 1999; *Cosgrove et al.*, 2003; *Chen et al.*, 2007]. Two long-term gridded China Meteorological Forcing Data Sets are available for the central TP. One was developed at the Institute of Tibetan Plateau Research, Chinese Academy of Sciences (http://dam.itpcas.ac.cn/data/User_Guide_for_China_Meteorological_Forcing_Dataset.htm; *Yang et al.*, 2010; hereafter ITPCAS). It covers the period of 1981–2008 at a $0.1° \times 0.1°$ grid with temporal resolution of 3 h. The observations collected at 740 operational stations of the China Meteorological Administration are merged into the corresponding Princeton meteorological forcing data [*Sheffield et al.*, 2006] to produce near-surface air temperature, pressure, wind speed, and specific humidity. The other was developed at the Beijing Normal University (http://globalchange.bnu.edu.cn/; *Li et al.*, 2014; *Huang et al.*, 2013; hereafter BNU). It covers the period of 1958–2010 on a 5 km grid with temporal resolution of 3 h. They used the spline and residual correction approach to merge observational, reanalysis, and remote sensing data for mapping near-surface air temperature, pressure, humidity, precipitation, wind speed, and shortwave and longwave radiations.

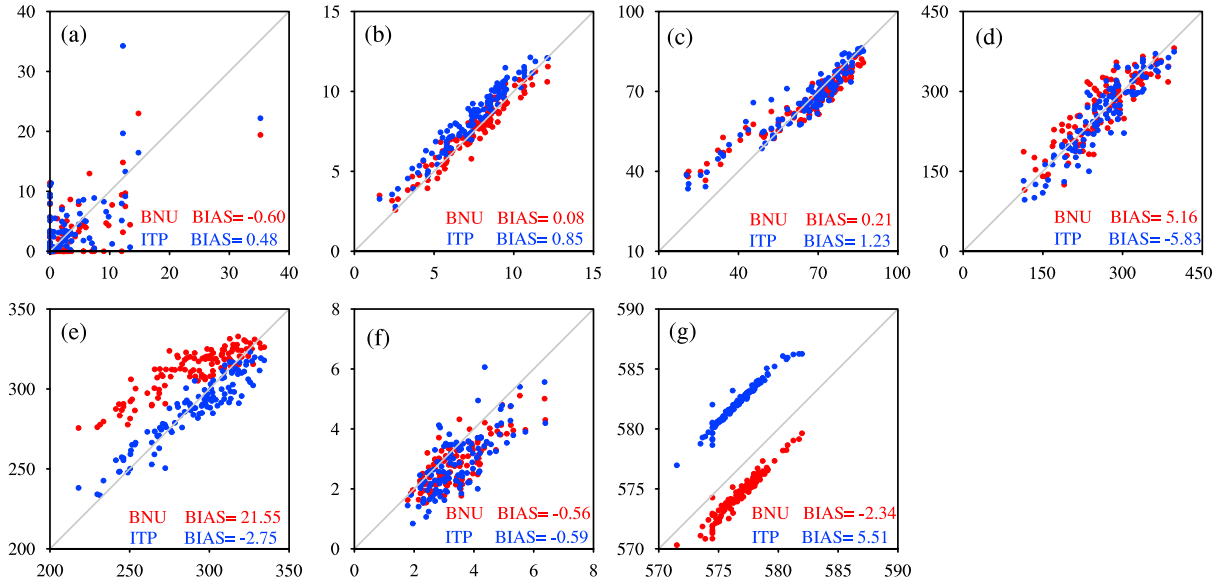

Figure 2. Comparing seven forcing variables between ITP/BNU (*Y* axis) and site observations (*X* axis) from 26 May to 16 September at Amdo. They are daily mean including nighttime values for (a) precipitation (mm d^{-1}), (b) surface air temperature (°C), (c) relative humidity (%), (d) downward shortwave radiation (W m^{-2}), (e) downward longwave radiation (W m^{-2}), (f) wind speed (m s^{-1}), and (g) surface pressure (hPa), respectively.

These two gridded data sets are compared with on-site observations from May to September 1998 (Figure 2). Both data sets have comparable abilities to capture the variability of the seven forcing variables in the measurement period. BNU/ITPCAS slightly overestimates the longwave radiation/surface pressure. Given the finer resolution of BNU over ITPCAS, we combined the near-surface air temperature, precipitation, pressure, wind speed, specific humidity, and shortwave radiation from the BNU and the longwave radiation from the ITPCAS as the forcing data at Amdo site.

2.4. Noah-MP Experiments

Eight Noah-MP simulations, documented in Table 3, were conducted to evaluate impacts of soil structures and processes. Before the simulation of 1998, a 30 year spin-up simulation was conducted with the combined gridded 1997 forcing to ensure the soil equilibrium state in all experiments but In Situ. The values of soil-state variables after the equilibrium, valid on 1 January 1998, were then used to initialize Noah-MP for simulation in 1998 in the former six experiments. CTL used a single, uniform soil texture in the entire soil column. LAY, compared to CTL, was designed to assess the impact of heterogeneity in the vertical soil texture profile. SOM assessed the impact of the soil organic matter at the topsoil layer. Root-s (Root-1, Root-2, and Root-3) evaluated the effect of the vegetation roots.

To investigate the soil-state initialization impact, simulations using the spun-up initiation (Root-3) are compared to In Situ that used observed soil moisture and temperature valid on 26 May 1998 to initialize soil-state variables (i.e., without spin-up and the simulation length is from May to September in In Situ). The former seven experiments used in situ observed forcing from 26 May to 16 September replacing the combined

Table 3. Noah-MP Numerical Experiments

	Model Physics	Atmospheric Forcing
CTL	Uniform column soil texture	Combine gridded forcing for 1 January 1997 to 25 May 1998 and in situ measurements for 26 May to 16 September 1998
LAY	Layered soil texture	Same as in CTL
SOM	Soil organic matter at topsoil based on Exp.2	Same as in CTL
Root-1	Rhizosphere at topsoil (Ks*10^{-1})based on Exp.3	Same as in CTL
Root-2	Rhizosphere at topsoil (Ks*10^{-2})based on Exp.3	Same as in CTL
Root-3	Rhizosphere at topsoil (Ks*10^{-3})based on Exp.3	Same as in CTL
In Situ	The same as Exp.4	No spin-up, using in situ measurements for 26 May to 16 September 1998
Grid	The same as Exp.4	Gridded forcing for 1 January 1998 to 16 September 1998

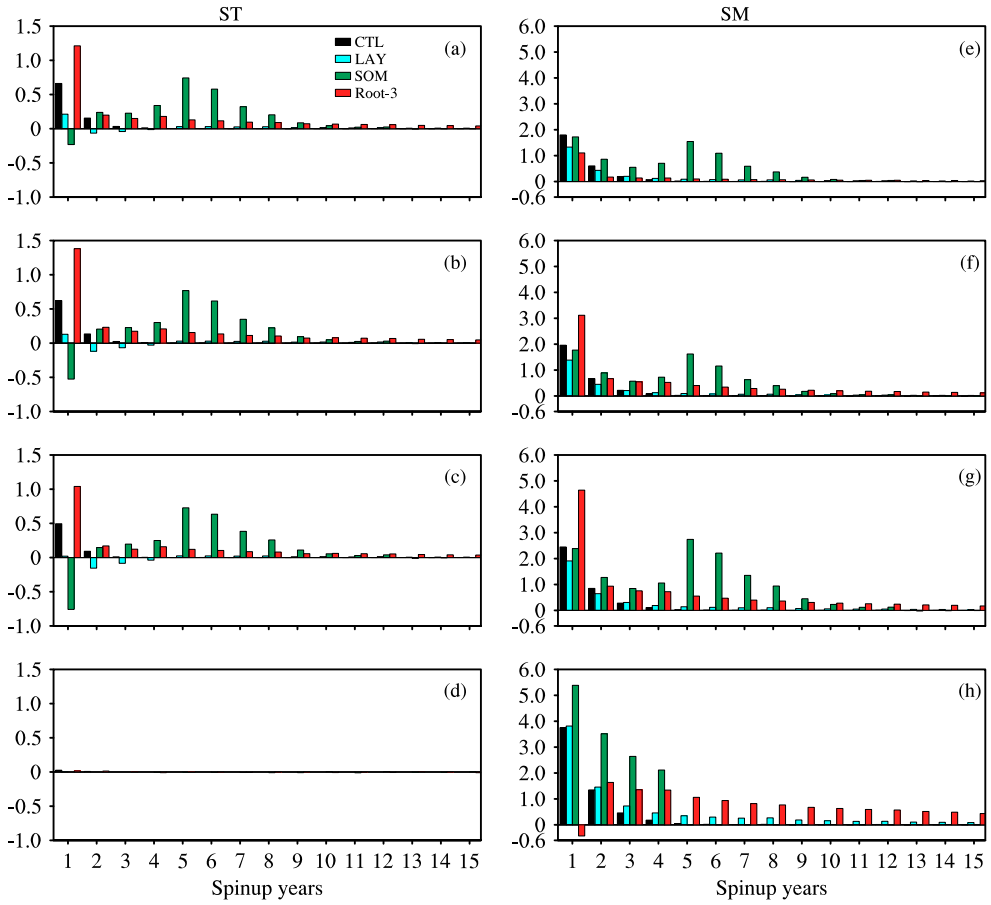

Figure 3. Spin-up time of (a–d) soil temperature (ST in °C) and (e–h) soil moisture (SM in %) for CTL, LAY, SOM, and Root-3.

gridded forcing, but the last one (Grid) used the combined gridded forcing from 1 January to 16 September 1998 to explore the influence of the forcing data at different scales.

3. Results and Discussions

3.1. Impacts of Soil Processes on Noah-MP Model Spin-Up

Cosgrove et al. [2003] utilized two extreme initial soil-moisture values (saturated and completely dry) and found that three LSMs investigated reached a state of rough equilibrium within the first 1 to 2 years. *Chen and Mitchell* [1999] found that, based on results of Noah-LSM 1° global simulations, the equilibrium conditions were established within 3 years over most areas. They indicated that in some regions with a deep soil layer and sparse vegetation, the equilibrium process took longer because the evaporation was limited by slow water diffusion time scales between the surface and deep soil layers.

The Amdo site is located in a permafrost region with an elevation about 4700 m. For the Noah-MP parameterizations used here, roughly a 4 year spin-up time was needed when using the default four soil layers with homogeneous column soil texture in CTL (Figure 3), compared to 3 year spin-up over most low-altitude areas [*Chen et al.*, 2007]. This suggests a slightly longer spin-up time due to the cryosphere processes at high altitude. However, LSM spin-up time significantly increases with the complexity of the soil vertical heterogeneity: 4 years at the topsoil but 10 years at the bottom of soil when heterogeneous soil texture is considered in LAY and up to 11 years when the organic matter is taken into account in SOM. Finally, it could take up to 15 to 30 years at the top/bottom layer to reach equilibrium in Root-s with spare to dense rhizosphere.

After the Noah-MP LSM reaches equilibrium, simulated soil temperature (ST), SLW, and total moisture content (SM, liquid SLW plus soil ice) on 26 May 1998 are listed in Table 4. The spun-up ST is generally close to observations but is slightly underestimated at two middle layers (1–3°C) and slightly overestimated in the topsoil

Table 4. States of Four Variables (ST: Soil Temperature; SM: Soil Moisture; SLW: Soil Liquid Water Content; TG: Ground Temperature) for Observations and Simulated Statements for CTL, LAY, SOM, Root-1, Root-2, and Root-3 at 26 May 1998 as the Initialization of 1998 Simulation

	Layer	Obs	CTL	LAY	SOM	Root-1	Root-2	Root-3
ST	1	281.8	281.1	281.2	280.9	281.2	281.2	281.3
	2	280.2	279.1	278.4	278.0	277.9	277.5	277.7
	3	276.3	274.3	273.2	273.2	273.2	273.2	273.2
	4	272.8	273.1	273.0	273.0	273.0	272.9	272.7
SM	1	-	0.19	0.18	0.26	0.20	0.15	0.15
	2	-	0.23	0.22	0.27	0.29	0.29	0.24
	3	-	0.26	0.25	0.32	0.35	0.37	0.26
	4	-	0.29	0.33	0.39	0.39	0.39	0.35
SLW	1	0.21	0.19	0.18	0.26	0.20	0.15	0.15
	2	0.21	0.23	0.22	0.27	0.29	0.29	0.24
	3	0.20	0.26	0.20	0.09	0.12	0.13	0.12
	4	0.21	0.11	0.09	0.09	0.09	0.09	0.09
TG		278.6	281.5	281.6	281.2	281.6	281.7	281.7

layer (0.5–1°C). At the bottom layer, all simulation results compared well with observations with negligible biases (0.1–0.3°C). For the top and bottom layers, the smallest bias occurs in Root-3, but CTL produces smallest bias for the two middle layers.

SLW is generally underestimated except for the second layer. Largest underestimation exists at the bottom layer following with the third layer. The large underestimation in SLW at the two bottom layers are likely related to the underestimation of ST which is below the freezing point, and most soil moisture was converted from liquid water to ice. The soil water, percolated from the topsoil, is stored in soil ice, leading to a slight overestimation in SLW at the second layer. Larger bias suggesting the organic matter plays a role there. Overestimation of SLW is also shown at the second layer in SOM, Root-1, Root-2, and at the top layer in SOM, which corresponds to a higher SLW, indicating that the organic matter does increase the SLW by increasing the porosity. Root-3 holds the SLW at the topsoil and reduces the overestimation at the second layer leading to a relative small bias.

It is also useful to examine simulated soil-ice content. Since the ST at the third layer is approximately the freezing point and above the freezing point at two upper layers, soil ice only exists in the bottom two layers. Ice fraction, denoting that the ice content divided the total SM, is 0.0% (62.1%), 20.0% (72.7%5), 71.9% (76.9%), 65.7% (76.9%), 64.9% (76.9%), and 53.8% (74.3%), respectively, for the third (fourth) layer. As above mentioned, the soil ice at the third layer closely follows the ST simulation. CTL produces ST 1° above the freezing point with zero ice fractions. Other experiments produce ST near the freezing point at the third layer with less than ¼ soil ice fractions. At the bottom layer, all experiments produce a lower ST than that at the third layer with more than 60% ice fractions. Other five experiments produce more ice than CTL, suggesting a great impact of the vertical heterogeneity on the ice-fraction simulation. Consistent with the SM, SOM, and Root-1, Root-2 simulates more ice fraction at two low layers than other experiments, due to the lower ST. Taking the SLW into account, we find that the relatively larger SM simulated in SOM, Root-1, and Root-2 are decomposed into the SLW at two upper layers when the ST is above the freezing point and into the soil ice at two bottom layers when the ST is below the freezing point. The increases in soil ice at the two bottom layers in SOM, Root-1, and Root-2 are due to lower ST causing the underestimation in the SLW. Unlike the ST, all experiments overestimate the ground temperature by about 3°C. The canopy water, snowpack depth, and snow water equivalent are zero at this site in the late May (not listed).

3.2. Impact of Soil Structures and Processes in the Monsoon Season

Consistent with *Yang et al.* [2005], the default Noah-MP simulation greatly underestimates the topsoil SLW in the monsoon season (CTL in Figure 4e and Table 5), a common problem in land model simulation in TP [*Yang et al.*, 2009; *Chen et al.*, 2012]. As shown in Figure 4, adding vertical heterogeneity in soil texture (LAY) makes such an underestimation slightly worse. Including organic matter (SOM) in Noah-MP does, to some extent, reduce the underestimation. However, including rhizosphere (Root-s) substantially reduces the dry bias in the topsoil SLW and the Root-3, in particular, agrees with the OBS well (Table 5 and Figure 4e). More significant improvements occur after July where the daily bias is reduced from $-11.9\,m^3\,m^{-3}$ in CTL to

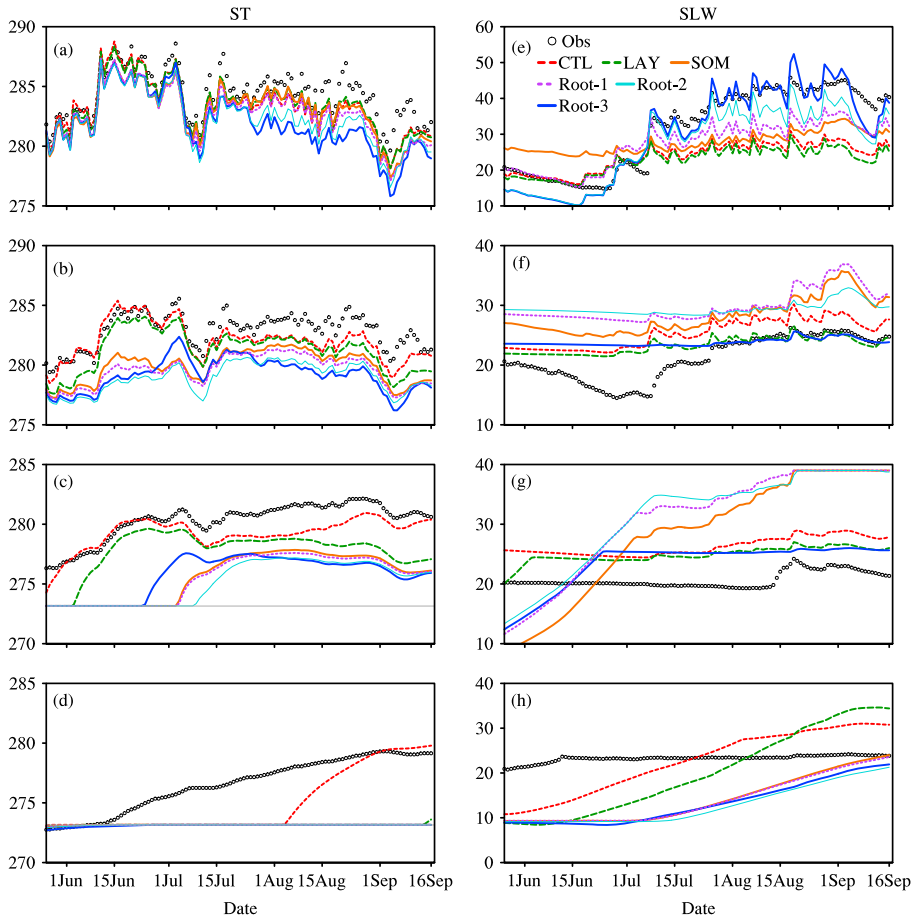

Figure 4. Variations of the daily mean (a–d) soil temperature (ST in K) and (e–h) soil liquid water content (SLW in %) at (Figures 4a and 4e) 5 cm, (Figures 4b and 4f) 25 cm, (Figures 4c and 4g) 75 cm, and (Figures 4d and 4h) 150 cm soil depth for 26 May to 16 September 1998 for the observation and CTL, LAY, SOM, Root-1, Root-2, and Root-3.

$-0.4\ m^3\ m^{-3}$ in Root-3, and root-mean-square error (RMSE) is reduced from $13.0\ m^3\ m^{-3}$ in CTL to $3.5\ m^3\ m^{-3}$ in Root-3, primarily due to the third-order reductions in the saturated conductivity at Amdo. This substantial improvement after July suggests a more dominant role of vegetation roots in SLW simulation in the monsoon season. SOM and Root-s produce an overestimation in SLW at the third layer and underestimation at the fourth layer below 1 m due to the organic matter impact. Roots in Root-3 hold more topsoil SLW (Figure 4e) and reduce the amount of soil water percolating to lower layer, leading to a good agreement between model results and observations at the second and third layers (Figures 4f and 4g).

All experiments underestimate ST from the top to the bottom layers in the monsoon season (Figures 4a–4d). The underestimation at the second and third layers might relate to the initiation of soil-state variables after spin-up that will be further discussed in section 3.4. Given the good performance of Root-3, we will focus on the results of Root-3 in the following sections, and the difference between Root-s and SOM is accepted as the root impact at this site.

Simulated differences in topsoil ST and SLW led to substantial differences in simulated surface energy and mass exchanges as shown in Figure 5 due to modifications in temperature and moisture gradients between land surface and near-surface air. CTL, LAY, and SOM overestimate the surface sensible heat fluxes but greatly underestimate latent heat fluxes in the monsoon season (Figures 5b and 5c). The low latent heat fluxes and high sensible heat fluxes in CTL, LAY, and SOM could be attributed to the dry biases in the topsoil SLW. Root-3 improves biases in the sensible heat and latent heat fluxes (Figures 5b and 5c). Biases in the latent heat flux are substantially reduced (Table 5). Remarkably, it better depicts the trend of increasing latent heat fluxes (Figure 5c) and decreasing sensible heat fluxes (Figure 5b) from the dry season to the monsoon season.

Table 5. Bias and RMSE of the Soil Temperature (ST) and Soil Liquid Water Content (SLW) for Eight Experiments Compared to the Observation From 26 May to 16 September

		SLW				ST			
	Layer	1	2	3	4	1	2	3	4
CTL	BIAS	−7.7	4.2	5.6	−0.7	−1.0	−0.9	−1.0	−1.6
	RMSE	10.9	4.6	5.7	6.3	1.3	1.2	1.4	2.3
LAY	BIAS	−8.8	2.2	4.2	−3.2	−1.0	−1.6	−2.5	−3.4
	RMSE	12.0	3.5	4.4	9.2	1.2	1.8	2.7	4.0
SOM	BIAS	−3.8	7.1	7.7	−9.3	−1.4	−3.0	−4.7	−3.4
	RMSE	9.5	7.3	12.0	10.4	1.7	3.1	4.8	4.0
Root-1	BIAS	−4.2	8.7	10.2	−9.4	−1.7	−3.3	−4.8	−3.4
	RMSE	7.0	9.0	13.0	10.4	1.9	3.4	4.9	4.0
Root-2	BIAS	−4.2	8.3	10.7	−10.5	−2.1	−3.9	−5.1	−3.4
	RMSE	5.3	8.9	13.1	11.1	2.4	4.0	5.3	4.0
Root-3	BIAS	−1.5	2.7	2.9	−10.0	−2.4	−3.7	−4.6	−3.4
	RMSE	3.9	4.2	4.7	10.9	2.8	3.8	4.7	4.0
In Situ	BIAS	−1.3	−1.3	−1.4	−2.8	−1.7	−1.1	0.3	2.9
	RMSE	3.5	3.3	1.8	3.0	2.2	1.5	0.7	3.0
Grid	BIAS	−2.6	2.6	2.9	−9.7	−1.8	−3.2	−4.3	−3.4
	RMSE	8.1	4.4	4.6	10.6	2.3	3.4	4.5	4.0

Consistent with the seasonal variability, Root-3 shows improvements in the monthly diurnal cycle of the latent heat flux and sensible heat flux (Figures 6b and 6d).

The Bowen ratio is the ratio of sensible heat fluxes to latent heat fluxes. Depending on the surface conditions, the Bowen ratios range from above 10 over the desert down to less than 0.1 over the ocean [*Bowen*, 1926; *Lewis*, 1995]. In general, 2 is the division between the semiarid and semihumid landscape, so the Bowen ratio

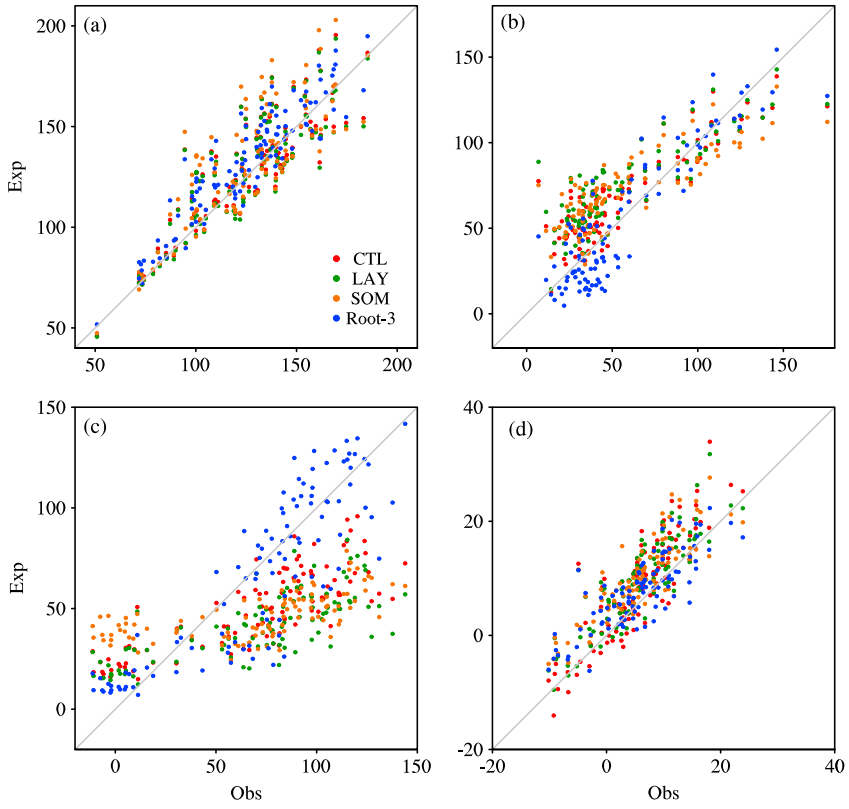

Figure 5. Scatterplots of the daily-averaged (a) surface net radiation and (b) sensible, (c) latent, and (d) ground heat fluxes (W m^{-2}) for CTL, LAY, SOM, and Root-3versus the observation from 26 May to 16 September 1998.

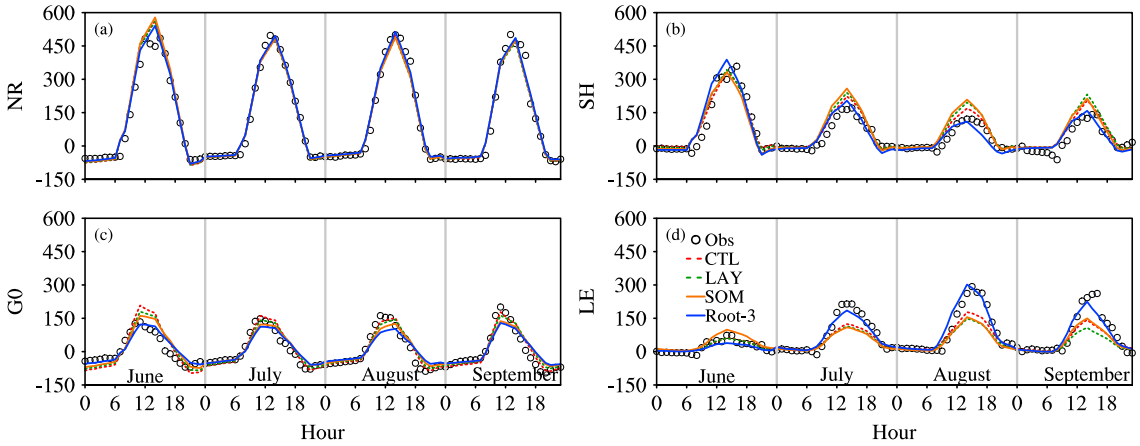

Figure 6. Monthly diurnal cycle for June, July, August, and September of (a) surface net radiation (NR in W m^{-2}), (b) sensible heat flux (SH in W m^{-2}), (c) ground heat fluxes (G0 in W m^{-2}), and (d) latent heat flux (LE in W m^{-2}). Hours are in local standard time.

is also used to illustrate the evolution between the dry and wet seasons [*Zhang et al.*, 2014c]. Compared to the large Bowen ratio in the transient season, Root-3 better depicts the Bowen ratio variations from the dry season to the wet season (Figure 7).

In general, biases in simulated ground heat fluxes are slightly improved in Root-3 as compared to CTL, LAY, and SOM (Table 6) as well. CTL, LAY, and SOM match the ground temperature well, but Root-3 increases the bias by 1°C. Note that when the Chen97 [*Chen et al.*, 1997] surface-layer parameterization scheme is used in Noah-MP, CTL, LAY, and SOM overestimate the ground temperature but Root-3 produces better results. This demonstrates that the bias in the ground temperature is highly related to the surface exchange parameterization and the treatment of thermal roughness length as indicated by *Chen and Zhang* [2009] and *Yang et al.* [2011], which would be an interesting subject to explore in future studies.

Daily surface runoff generally followed the variability of the precipitation more closely in the monsoon season (Figures 8a and 8c) than that in transient season (Figure 8b) due to frozen ground physics in the latter. Also, it is better correlated with precipitation than with subsurface SLW in all experiments. When the same precipitation forcing is used as CTL, LAY, SOM, and Root-3, larger surface runoff in these simulations (Figure 8a) corresponds to smaller topsoil SLW in Figure 4. However, subsurface runoff shows a clear correlation with subsurface SLW. CTL, LAY, and SOM produce a relative larger subsurface runoff than Root-3 (Figure 8d). Large subsurface runoff in CTL, LAY, and SOM is clearly related to the overestimation in the SLW at subsurface layers as shown in Figures 4f–4h, which in turn is related to the thawing at subsurface layers (Figures 4c and 4d).

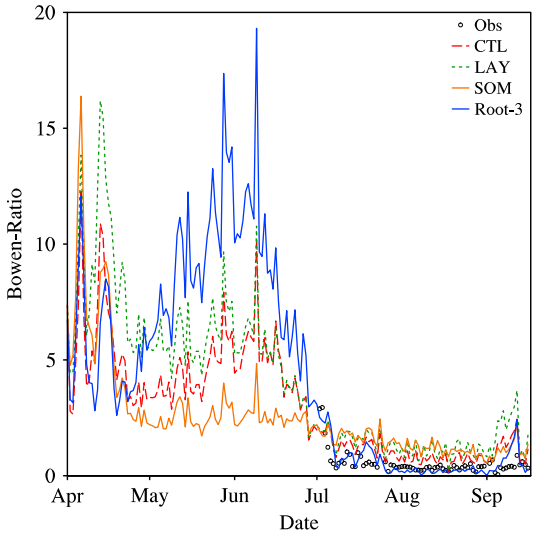

Figure 7. Comparing simulated Bowen ratio from CTL, LAY, SOM, and Root-3 with observation from 26 May to 16 September.

3.3. Impact of Soil Parameterizations in the Transient Season

Differences in model results during the monsoon season discussed above are certainly related to the evolution of soil state in the transient season. Due to the lack of observations for the transient season (April–May), we focused on comparing different Noah-MP simulations to assess the impacts of the above soil processes on soil ice melting. Figure 9 shows the variability of SLW, soil ice, and ST for CTL, LAY, SOM, and Root-3 from 1 April to 31 May where soil ice thaws. Various soil processes had little impact on the evolution of topsoil temperature (Figure 9a) that increased above the freezing point

Table 6. Bias and RMSE of the Surface Net Radiation (NR); Skin Temperature (TG); and Sensible (SH), Latent (LE), and Ground (G0) Heat Fluxes for CTL, LAY, SOM, Root-3, In Situ, and Grid Compared to the Observation From 26 May to 16 September

	NR		G0		TG		SH		LE	
	BIAS	RMSE	BIAS	RMSE	BIAS	RMSE	BIAS	RMSE	BIAS	RMSE
CTL	4.1	14.9	2.9	5.3	−0.8	1.4	11.4	20.9	−20	34.3
LAY	2.6	15.2	3.9	5.5	−0.6	1.4	16.8	25.8	−27.7	41.9
SOM	6.3	18.6	4.3	5.8	−0.8	1.7	15.1	26.6	−23.2	42.8
Root-3	7.3	13.4	2.0	4.6	−1.8	2.1	−1.5	17.1	−3.1	22.1
In Situ	13.1	18.5	−4.0	5.7	−1.6	2.0	7.3	19.1	−0.6	24.6
Grid	3.1	28	2.2	6	−1.2	2.1	2.2	26.1	−12.1	34.4

on 7 April but substantially affected ST in deep soil layers. For instance, in the second soil layer, CTL first climbs above the freezing point, followed 4 days later by LAY, then followed 10 days later by Root-3, and finally followed 7 days later by SOM. For the deep fourth soil layer, LAY produced highest ST and Root-3 produces lowest ST.

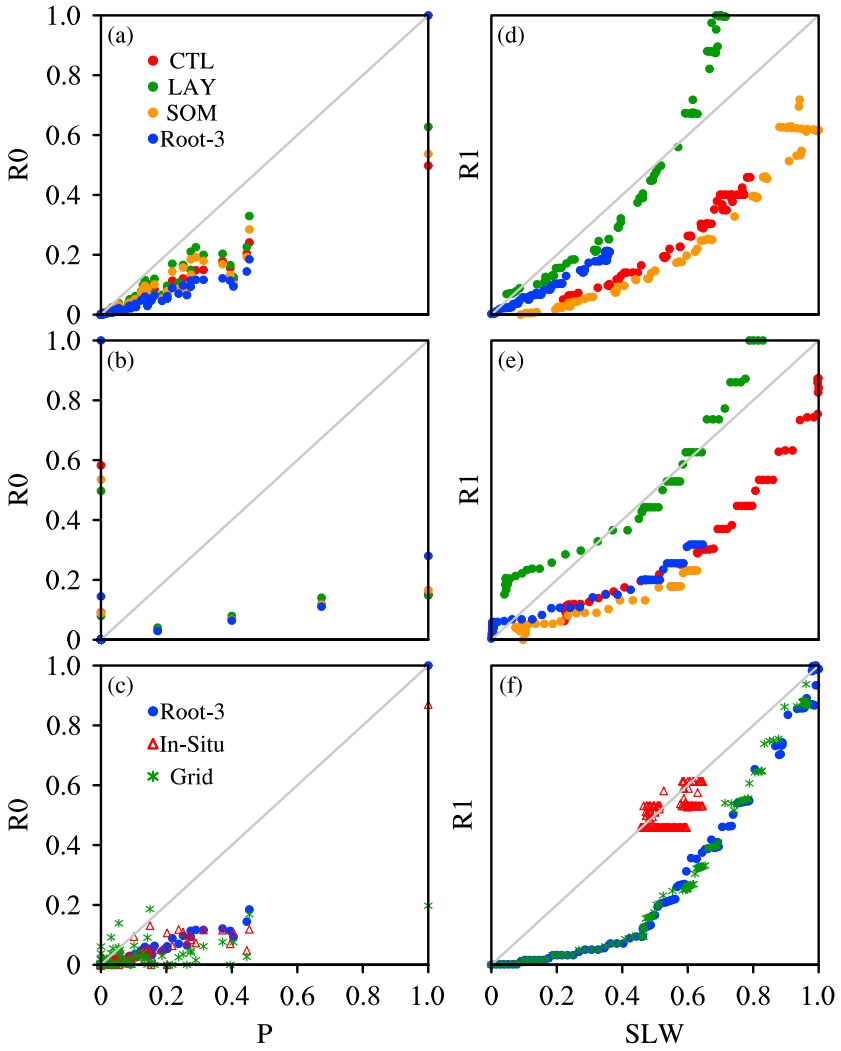

Figure 8. (a–c) Normalized surface runoff (R0) versus normalized precipitation (*P*) and (d–f) normalized subsurface runoff (R1) versus normalized subsurface SLW. Figures 8a and 8d are CTL, LAY, SOM, and Root-3 results in the monsoon season; Figures 8b and 8e are CTL, LAY, SOM, and Root-3 results in the transient season; and Figures 8c and 8f are Root-3, In Situ, and Grid results in the monsoon season. The subsurface SLW here is the average of the SLW except for the top layer. *P*, SLW, and runoff are normalized to 0–1 by (A-Amin)/(Amax-Amin).

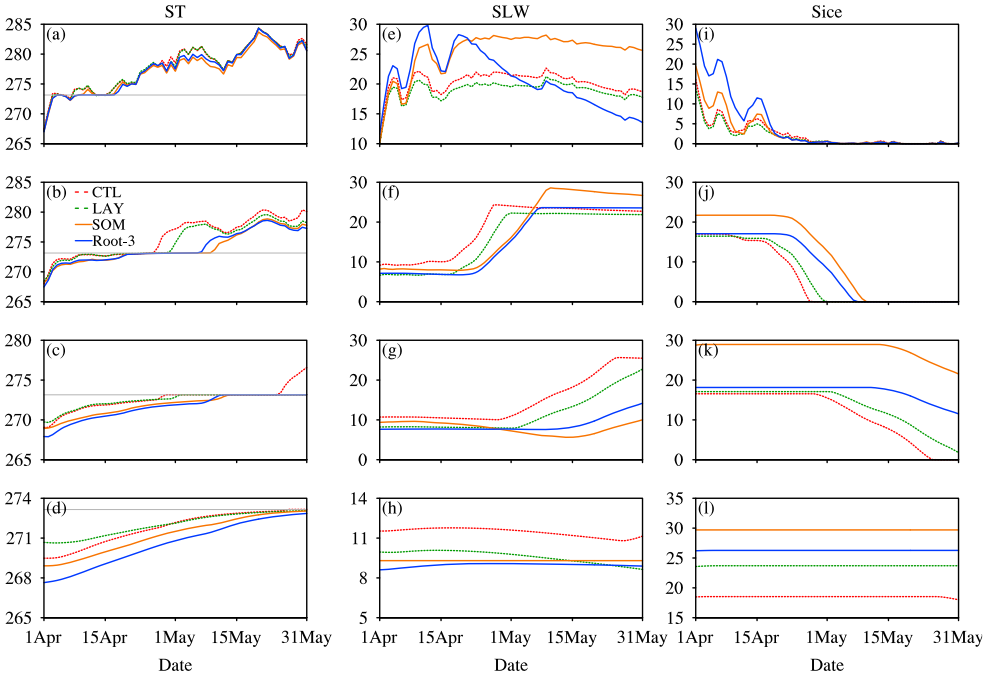

Figure 9. Daily mean (a–d) soil temperature (ST in K), (e–h) soil liquid water content (SLW in %), and (i–l) soil ice content (Sice in %) at (Figures 9a, 9e, and 9i) 5 cm, (Figures 9b, 9f, and 9j) 25 cm, (Figures 9c, 9g, and 9k) 75 cm, and (Figures 9d, 9h, and 9l) 150 cm soil depths from 1 April to 31 May 1998 simulated in CTL, LAY, SOM, and Root-3.

It is clear that the first-layer SLW evolution is mainly controlled by precipitation, soil hydraulic conductivity, and runoff, rather than by soil temperature (Figure 9e). Root-3 shows the largest seasonal amplitude because of high water-holding capacity in the shallow root zones for wetting and higher soil-ice fraction during freezing periods which reduce liquid soil moisture. SOM produced overly high soil moisture mainly due to its high soil porosity in the first layer.

It is also clear that the second-layer SLW evolution is highly correlated with ST evolution, because liquid soil moisture begins to increase after mid-April following the thawing soil ice (Figures 9b, 9f, and 9i) in each experiment. CTL wets earliest responding to the early thawing, and the layered soil texture in LAY delays the thawing by about 3 days. Higher second-layer SLW in SOM is largely due to higher ST and greater percolation from its higher first-layer SLW, because soil hydraulic conductivity is increased in organic matter (Figure 9e). Although the rhizosphere effect is only parameterized for the topsoil, it affects the second layer due to the movements of the SLW between soil layers.

Soil temperature at the third layer is below the freezing point except for CTL by the end of May, so significant soil ice exists throughout the transient season (Figure 9k). However, liquid water exists even in subfreezing temperature in all soil layers due to the treatment of supercooled liquid water (SLW) and fractional soil ice in Noah-MP [*Niu et al.*, 2011]. SLW in CTL increases to its highest values by the end of May due to the start of the melting phase and higher soil moisture in the first and second layers. However, before ST becomes higher than the freezing point, SLW keeps increasing from the beginning of the May, mainly due to the percolation of soil water from the second layer where soil ice melts earlier (Figures 9f and 9i).

SLW in the third soil layer in CTL and LAY are substantially greater than that in SOM and Root-3 (Figure 9g), suggesting that more SLW is held in the two upper layers (Figures 9e and 9f) because the organic matter enlarges the porosity and roots reduce their hydraulic conductivity. The bottom layer (Figures 9d and 9h) is similar to the third layer.

Therefore, generally, the seasonal variations in SLW are highly correlated with ST simulation because of the freeze-thaw cycle. Low thermal conductivity in organic matter in SOM produces lower soil temperature throughout the soil column, consistent with results of *Lawrence and Slater* [2008]. In Root-3, low hydraulic

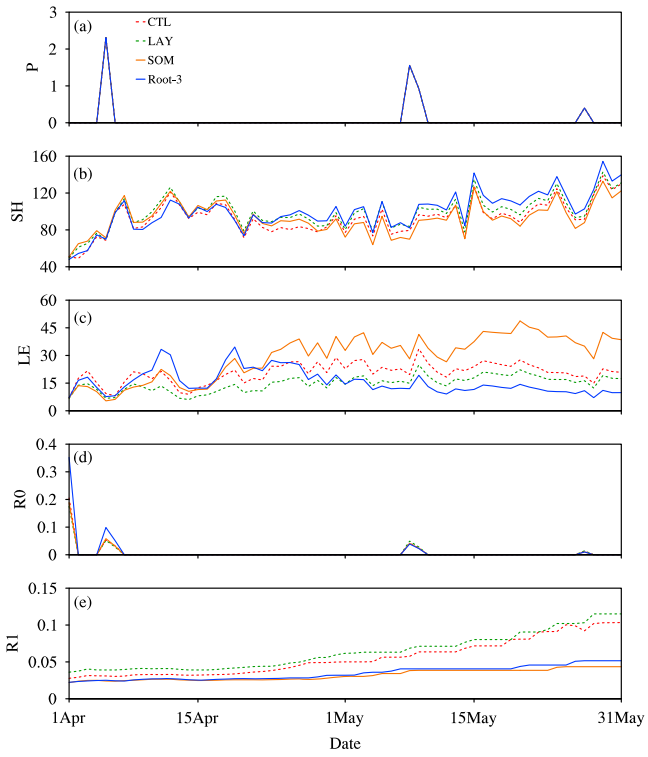

Figure 10. Variations of the daily (a) precipitation (*P*, unit: mm d^{-1}), (b) sensible heat flux (SH, unit: W m^{-2}), (c) latent heat flux (LE, unit: W m^{-2}), and (d) surface and (e) subsurface runoff (R0 and R1, unit: mm d^{-1}) from 1 April to 31 May 1998 for the observation (Obs), CTL, LAY, SOM, and Root-3.

conductivity reduces soil moisture in deeper layers and hence reduces thermal conductivity, leading to lower soil temperatures as well. Lower ST results in higher fractions of soil ice and lower SLW in SOM and Root-3 (Figures 9d, 9h, and 9l).

Figure 10 shows variations of surface heat fluxes and hydrologic components for CTL, LAY, SOM, and Root-3 in the transient season. The greatest difference across experiments lies in the latent heat flux (Figure 10c), which is highly correlated with the SLW variations in the topsoil (Figure 9e). The SOM produced highest topsoil SLW and latent heat flux after thawing because of greater porosity in organic soils. Although SM in Root-3 in April is lower than that in SOM, the saturation levels are relatively higher than Root-3 due to lesser porosity in Root-3 to produce higher latent heat flux. The variability pattern in the sensible heat flux is the opposite of the latent heat flux, but differences in the sensible heat flux between experiments are smaller compared to the latent heat flux.

The other pronounced difference between simulations is the simulated subsurface runoff, especially in May (Figure 10e), which is highly correlated with subsurface SLW (Figure 8e). CTL and LAY produce higher bottom layer SLW and hence greater subsurface runoff than SOM and Root-3. Simulated surface runoff is nearly identical among experiments, which is essentially controlled by the precipitation and surface infiltration rate. Small amounts of intermittent precipitation (Figure 10a), along with a large fraction of impervious soil in early April (Figures 9a–9d), generate low surface runoff. Root-3 produced relatively higher surface runoff than CTL, LAY, and SOM due to its low hydraulic conductivity.

3.4. Uncertainties in the Initialization of State Variables

Two methods are commonly used to initialize land-surface models: (1) using directly observed soil moisture, soil temperature, and snow and (2) using spun-up soil conditions from long-term off-line LSM simulation/assimilation, because the observations alone may not provide the necessary information for LSM initialization or each LSM may have its own climatology [*Koster and Milly*, 1997]. So far, we have discussed experiments with spun-up soil conditions. In this section, we now assess the results using direct observations

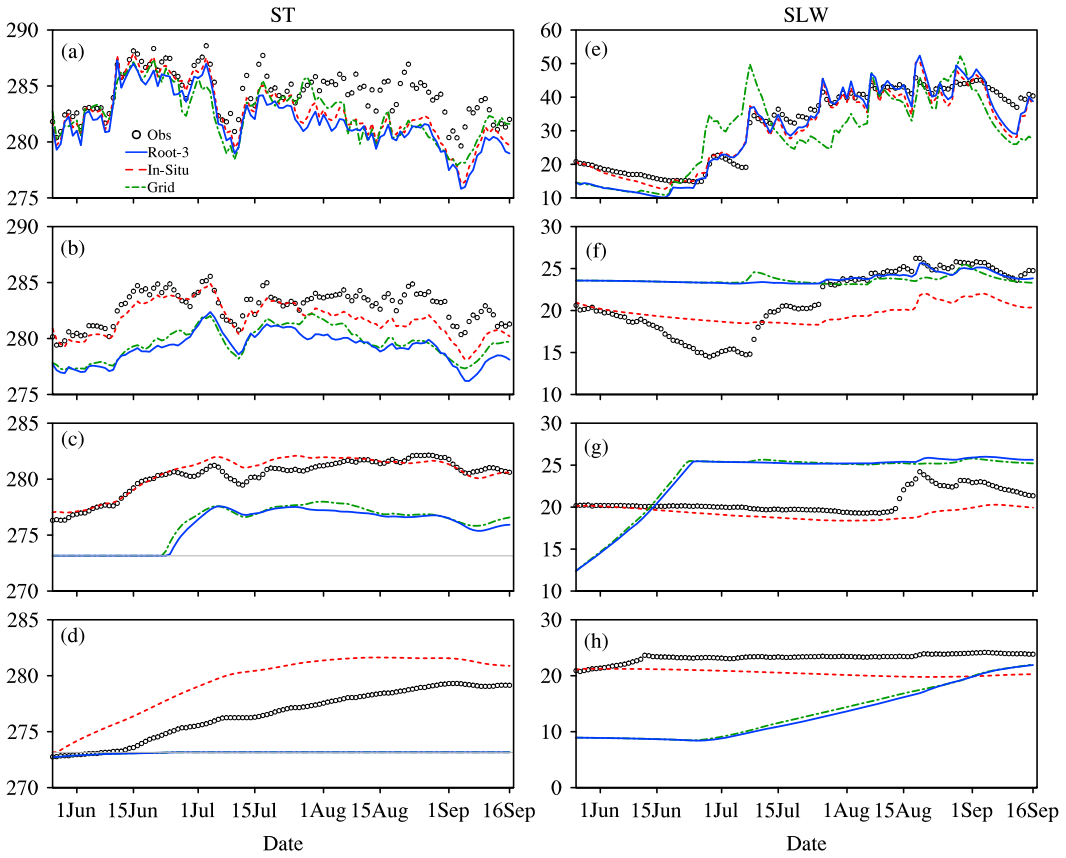

Figure 11. Variations of daily mean (a–d) soil water content (SLW in %) and (e–h) soil temperature (ST in K) at four soil depths from 26 May to 16 September 1998 for the Obs, Root-3, In Situ, and Grid.

as soil initial conditions. Root-3 and In Situ are all forced by the site observations from 26 May to 16 September, so the differences between those two simulations are solely caused by initial soil conditions on 26 May: Root-3 using spun-up ST and SLW conditions and In Situ using the observed ST and SLW.

The topsoil ST in Root-3 and In Situ is similar and underestimated (Figure 11a). Thus, the general trend of underestimating ST came from the parameterizations, not the initiation. At two middle soil layers, however, significant differences in ST between Root-3 and In Situ on May 26 have a long memory to influence ST in the following months. While Root-3 underestimated ST, In Situ agreed with observations very well. The low bias in ST is reduced from −2.21°C in Root-3 to 0.32°C in In Situ in middle soil layers (Table 5). Clearly, underestimation of ST in Root-3 can be attributed to the underestimation of ST at the model initialization time.

At the bottom layer, Root-3 underestimated ST, but In Situ overestimated ST. Although In Situ overestimated the bottom soil ST (1.5 m below the ground surface), it reproduced the seasonal variations of observed ST better than Root-3 in which ST is rather stationary. This indicates an active bottom soil at this site, because higher ST in the third soil layer in In Situ transports greater heat than Root-3 downward to warm its bottom soil layer. Differences in ST between Root-3 and In Situ increased with the soil depth, indicating that deeper soils are more affected by the initialization than shallow soil layers.

Root-3 produced lower SLW in topsoil than In Situ in late May and early June but was similar to In Situ after mid-June (Figure 11e). In Situ produced lower SLW at two middle soil layers and higher SLW at the bottom layer than Root-3 but closer to observations (Figures 11f and 11g). These differences suggest substantial influences of SLW initialization, especially at deep soil layers. Both Root-3 and In Situ underestimated seasonal variability of SLW, whereas Root-3 showed a greater variability than In Situ. The mid-June rapid increase of the third soil layer SLW in Root-3 is closely associated with its simulated thawing in that layer.

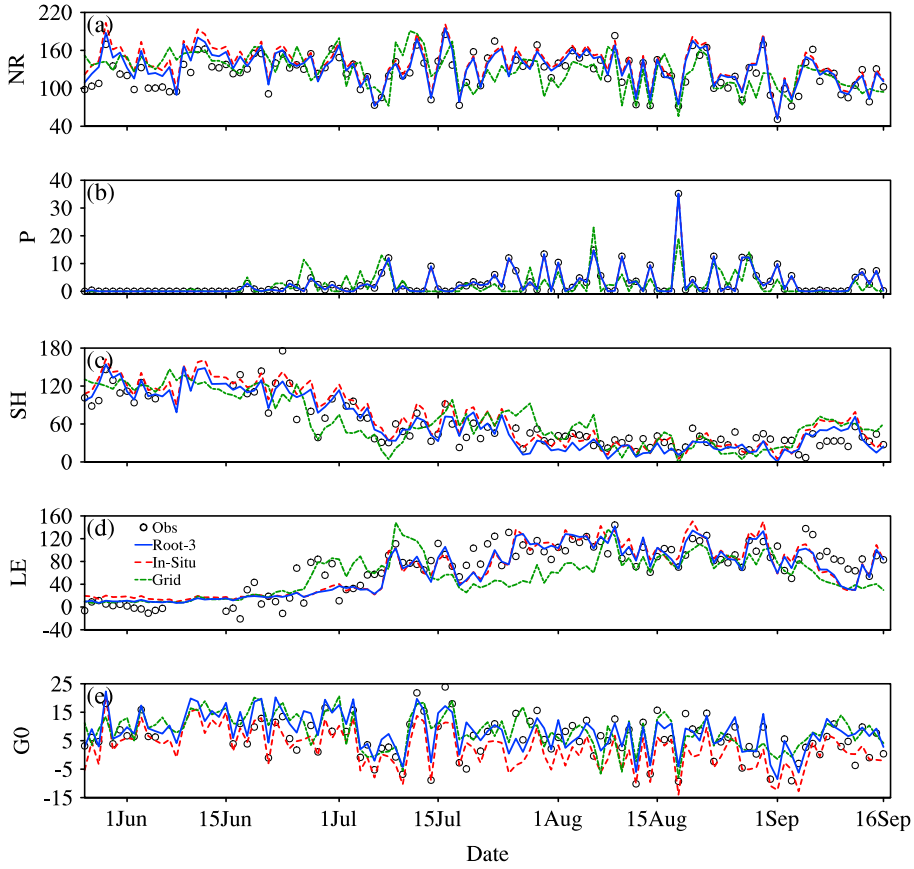

Figure 12. Daily (a) net surface radiation (NR, unit: W m^{-2}), (b) precipitation (*P*, unit: mm d^{-1}), (c) sensitive heat flux (SH, unit: W m^{-2}), (d) latent heat flux (LE, unit: W m^{-2}), and (e) ground heat flux (G0, unit: W m^{-2}) from 26 May to 16 September 1998 for the observation (Obs), Root-3, In Situ, and Grid.

Despite those differences in ST and SLW, little difference is found in net surface radiation, sensible heat flux, and latent heat flux between Root-3 and In Situ (Figures 12a, 12c, and 12d). The only noticeable difference is perhaps the ground heat flux (Figure 12e), and In Situ underestimated the ground heat flux (see also Table 6) due to its higher topsoil temperature than Root-3. Except for the ground heat flux, the other difference is simulated subsurface runoff (Figure 8f): In Situ shows a constant subsurface runoff due to a nearly constant SLW from 26 May to 16 September, but Root-3 shows an increasing subsurface runoff due to an increasing subsurface SLW. Despite the pronounced differences in the subsurface runoff simulation, Root-3 and In Situ generate a comparable surface runoff (Figure 8c) due to the identical precipitation. This again demonstrates that surface runoff is more correlated to the precipitation; however, the subsurface runoff is more correlated to the subsurface water content. In summary, soil initialization at this site has long memory to affect seasonal soil temperature and hydrologic components (soil moisture and runoff) in deep soil layers.

3.5. Uncertainties in Atmospheric Forcing Conditions

As shown in Table 3, combined gridded forcing (5 km horizontal resolution) from 1 January 1997 to 16 September 1998 is used as forcing in Grid. To test the sensitivity of the model physics, the gridded forcing from 26 May to 16 September 1998 was replaced with the in situ point measurements from Root-3. Hence, differences between Root-3 and Grid indicate the impact of forcing at different scales. Figure 11 illustrates that different scale forcings mainly affect the topsoil simulation results and elicit almost no difference in the deep soil. Grid shows greater seasonal variability in the topsoil ST and SLW than the Root-3, being cooler and wetter during 16 June to 15 July and warmer and dryer later which is consistent with the gridded forcing.

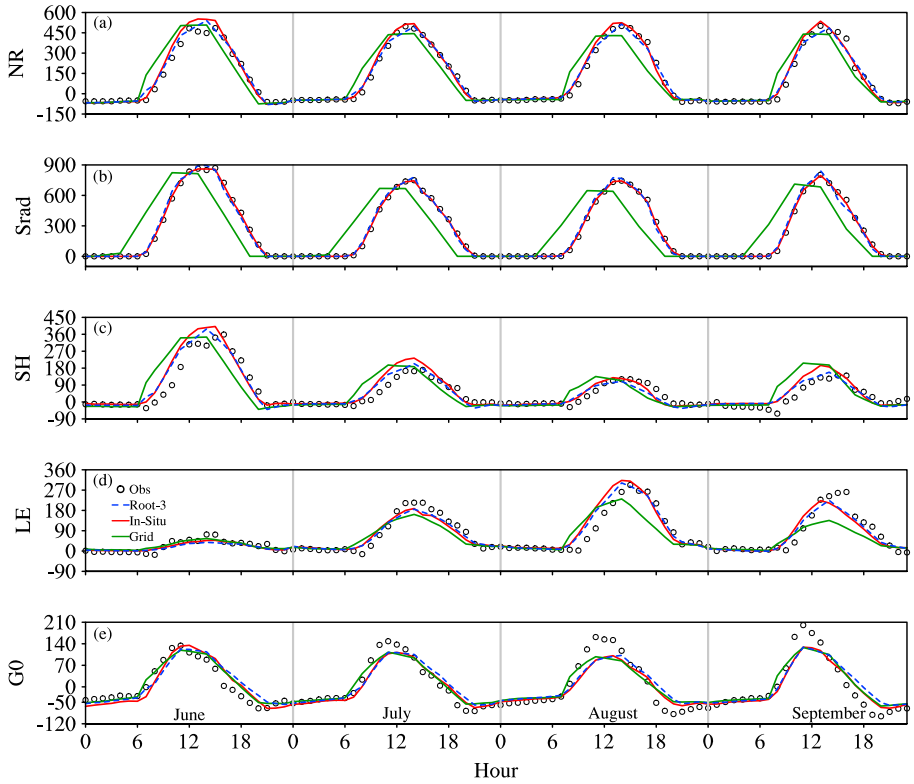

Figure 13. Variability of the daily (a) net surface radiation (NR, unit: W m^{-2}), (b) downward shortwave radiation (Srad, unit: W m^{-2}), (c) sensitive heat flux (SH, unit: W m^{-2}), (d) latent heat flux (LE, unit: W m^{-2}), and (e) ground heat flux (G0, unit: W m^{-2}) from 26 May to 16 September 1998 for the observation (Obs), Root-3, In Situ, and Grid.

Differences in topsoil ST and SLW modify the land-surface temperature and humidity gradients and consequently affect net radiation and sensible and latent heat fluxes (Figures 12 and 13 and Table 6). In general, Grid shows lower net radiation than Root-3, leading to a slightly lower ground temperature. The smaller net radiation in Grid occurred mostly during 18 July to 18 August; it is opposite in 18 June to 18 July. The smaller net radiation from 18 July to 18 August distributes into an even large smaller latent heat flux and a slight larger sensible heat (Figure 12). The monthly diurnal cycle only presented an underestimation in surface net radiation for Grid in the afternoon (Figure 13a); however, it is overestimated in the morning.

Low biases in the surface net radiation in Grid occurred in the afternoon (Figure 13a), primarily caused by lower downward solar radiation (Figure 13b). The morning net radiation is overestimated in Grid, which is again consistent with its shortwave radiation variations (Figure 13b). Moreover, the underestimation in the net radiation in the afternoon is mainly partitioned into latent heat fluxes in August and September (Figure 13d), but the overestimation in the net radiation in the morning is mainly partitioned into sensible heat fluxes all over the simulation period (Figure 13c).

In contrast to the impact of soil initialization, the impact of different scale forcings mainly affects surface variables. The seasonal variability of surface energy fluxes in Grid and Root-3 is mainly modulated by input precipitation (Figures 2a and 12b) and shortwave radiation (Figures 2d and 13b). This confirms that the precipitation and radiation forcings play an important role in the surface flux exchanges through the impact on the topsoil temperature and moisture, which could exert further impact on the weather prediction [*Trier et al.*, 2004, 2011; *Gao et al.*, 2004, 2008].

3.6. Accumulated Water Budget

Koster and Milly [1997] demonstrated that different LSMs exhibit substantially different climatology of the annual mean of soil moisture and the amplitude of the seasonal change of soil moisture owing to differences in treating evaporation and runoff as functions of soil moisture. The observed accumulation of precipitation (*P*) at this site is 313.4 mm from 26 May to 16 September (Figure 14a), and observed

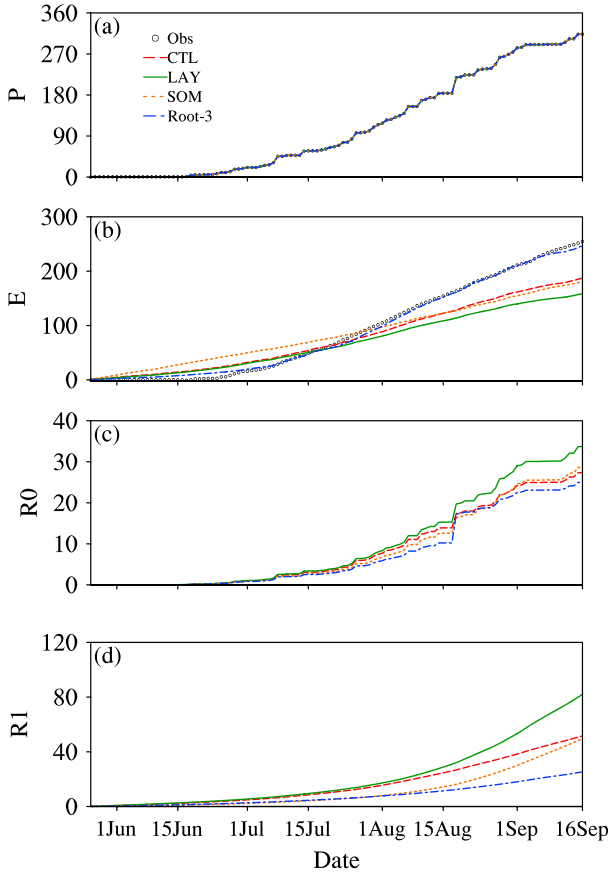

Figure 14. Comparison of accumulated (a) precipitation (*P*, unit: mm), (b) evapotranspiration (*E*, unit: mm), (c) surface runoff (R0, unit: mm), (d) and subsurface runoff (R1, unit: mm) from 26 May to 16 September for the OBS, CTL, LAY, SOM, and Root-3.

accumulation of evaporation (*E*) calculated from latent heat fluxes is 254.2 mm (Figure 14b). Thus, the estimated total runoff from *P-E* is 58.9 mm. Root-3 produced the highest accumulated *E* with 246.5 mm among four simulations, and LAY and SOM had relative low *E* ranging from 158.3 mm to 180.4 mm (Figure 14b). Including the rhizosphere with a larger water-holding capacity in Root-3 results in more topsoil SLW and higher *E* in the monsoon season. SOM has higher *E* after melting in May but lower *E* in the monsoon season, consistent with the greater topsoil SLW in the transient season and relative lesser topsoil SLW in the monsoon season. The difference between the largest and smallest bias in simulated *E* accumulation reaches 88.2 mm (36% of the *E* accumulation in Root-3) between LAY and Root-3. This suggests the uncertainty in simulated accumulated *E* from the soil structure and physics reaching 36% in LAY when compared to Root-3.

Consequently, lower *E* in LAY and SOM results in more runoff than Root-3. The higher runoff in LAY and SOM is proportionally distributed into surface and subsurface runoffs. LAY simulates the highest subsurface runoff due to the large infiltration from above layers (Figures 14c and 14d). Root-3 produces the lowest runoff accumulation owing to large *E*, especially low subsurface runoff because of the small SLW in the subsurface layers. Runoff ratio denoted as runoff dividing precipitation is 18.8%, 25%, 37%, 25%, and 16% for the OBS, CTL, LAY, SOM, and Root-3, respectively.

Soil initialization has minor impacts on the simulated evapotranspiration and surface runoff when comparing Root-3 to In Situ (Figures 15b and 15c) owing to the identical precipitation (Figure 15a) but mainly affects subsurface variables (Figure 15d) as discussed in section 3.4. However, the gridded forcing (Grid) has greater impact on the accumulate *E* and R0 due to different *P*. The accumulated gridded precipitation is 245.2 mm from 26 May to 16 September (Figure 15a), which is 68.2 mm less than the OBS, Exps6 and 7. Grid simulates 213.7 mm in the accumulated evapotranspiration (Figure 15b). It occupies 87% of the precipitation and smaller percentage runoffs, especially the surface runoff, than the OBS, Exsp6 and 7 (Figure 15c).

4. Summary

Land-surface models can build understanding of soil dryness/wetness by accurately simulating the evolution of soil moisture, evapotranspiration, and runoff over the TP region where observations are sparse. This study assesses the simulations with the new generation Noah-MP LSM conducted at the Amdo site in the central TP. The default Noah-MP gives large dry biases in topsoil moisture in the monsoon season, a common problem in previous LSM studies for this region. Using observed profiles of soil texture to replace the default, vertically uniform soil texture in Noah-MP, and representing organic matter in the model do not significantly improve the topsoil moisture simulation. Because the short-grassland roots in the central TP

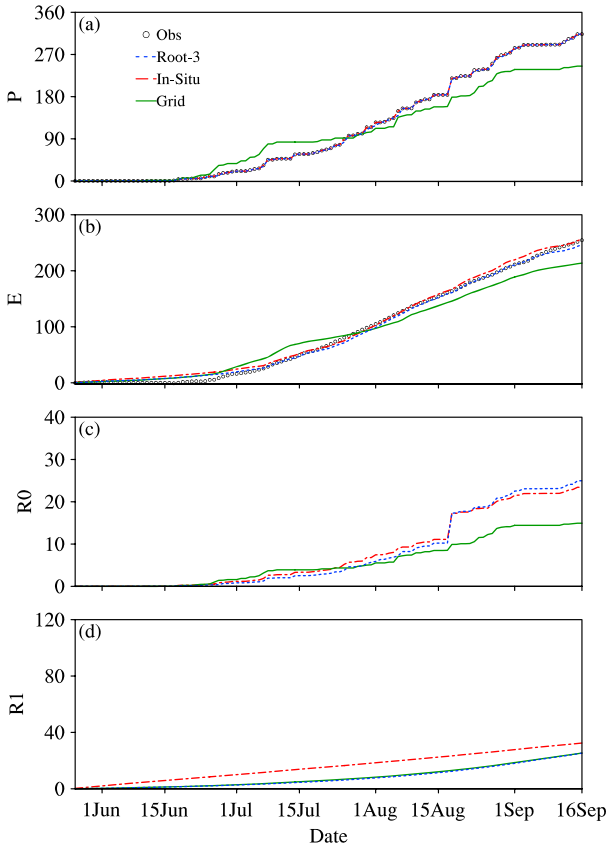

Figure 15. (a–d) The same as Figure 14 but for the OBS Root-3, In Situ, and Grid.

are mostly distributed underneath shallow soils, a number of sensitive experiments were conducted to explore the influence of the rhizosphere, along with impact of uncertainties in forcing conditions and initialization, on soil temperature, soil moisture, surface energy, and water cycles. The main findings are

1. The LSM spin-up time at the central TP depends heavily on the complexity of the model physics, ranging from 4 years with the simplest soil physics to 11–30 years with the addition of organic matter and spare to dense rhizosphere parameterization in Noah-MP.
2. The topsoil moisture is underestimated by about 50% in the default Noah-MP, but representing layered soil texture and organic matter does not improve much. However, such an underestimation is greatly reduced when the rhizosphere effect is taken into consideration. Reducing the saturated conductivity due to the mucilage in the rhizosphere at the topsoil produces better results. Impact of the rhizosphere could be illustrated as Figure 16. Surface sensible and latent heat fluxes are better simulated in the monsoon season as well. Adding layered soil texture and organic matter in Noah-MP retard the thawing in deep soil layers, and the rhizosphere effect delays thawing even more in the transient season.
3. Uncertainties in soil initialization significantly affect soil temperature and moisture in deep soils but have minimal influences on surface energy fluxes. Conversely, uncertainties in atmospheric forcing conditions mainly affect topsoil variables and consequently the surface energy fluxes, surface runoff, and evaporation. In general, at this site, uncertainties in forcing conditions seem to have more impact than uncertainties in soil initialization.
4. Model physics could cause up to 36% uncertainty in the accumulated evapotranspiration simulation in May to September 1998. Runoff ratio could be up to 2 times of the OBS. Subsurface runoff is more affected due to the differences in the subsurface SLW. Different forcing exerts greater impacts on evapotranspiration and surface runoff accumulation because of the precipitation differences. Subsurface runoff is seldom affected by the forcing.

This study highlights the significant effects of soil process uncertainties on Noah-MP simulated surface energy and water budgets, and including the rhizosphere parameterization helps improve model results. Nevertheless, the reduced Ksat is a sensitive test for the roots impacts which require further in situ

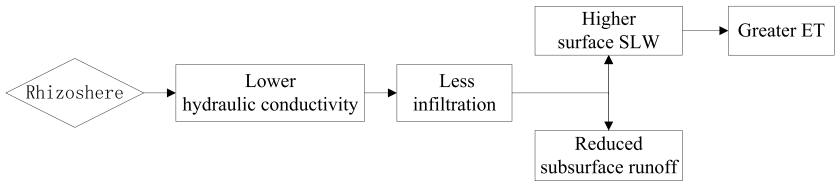

Figure 16. Flow chart of the impact of the rhizosphere.

measurements to confirm in the Third Tibetan Experiments. Moreover, using the 10^{-3} reduction in the hydrological conductivity in rhizosphere might not apply to other plant species or to other growing-season periods. *Carminati and Vetterlein* [2013] documented that the water-holding capacity varies with seasons, plant species, and growing conditions and decreases from the young roots to the old ones. Parameterizing the dynamic rhizosphere process, by considering the above factors, will certainly help a more realistic representation of this process in LSMs.

Acknowledgments
This work is jointly funded by the Ministry of Science and Technology of the People's Republic of China (2013CB956004), National Natural Science Foundation of China (91537211, 91537105, 41322033), and "100-Talent" program granted by the Chinese Academy of Sciences to Yanhong Gao. This study is also supported by the Water System Program at the National Center for Atmospheric Research. We appreciate the free access of the GAME Tibet data sets at http://wdcdgg.westgis.ac.cn/chinese/DATABASE/Game_Tibet/. Two forcing data sets are available at http://globalchange.bnu.edu.cn/ and http://dam.itpcas.ac.cn/data/User_Guide_for_China_Meteorological_Forcing_Dataset.htm.

References

Ball, J. T., I. E. Woodrow, and J. A. Berry (1987), A model predicting stomatal conductance and its contribution to the control of photosynthesis under different environmental conditions, in *Process in Photosynthesis Research*, vol. 1, edited by J. Biggins, pp. 221–234, Martinus Nijhoff, Dordrecht, Netherlands.

Baret, F., M. Weiss, R. Lacaze, F. Camacho, H. Makmara, P. Pacholczyk, and B. Smets (2013), GeoV1: LAI, FAPAR essential climate variables and FCOVER global time series capitalizing over existing products. Part 1: Principles of development and production, *Remote Sens. Environ.*, *137*, 299–309.

Barlage, M., M. Tewari, F. Chen, G. Miguez-Macho, Z.-L. Yang, and G. Y. Liu (2015), The effect of groundwater interaction in North American regional climate simulations with WRF/Noah-MP, *Clim. Change*, *129*, 485–498, doi:10.1007/s10584-014-1308-8.

Bolten, J. D., V. Lakshmi, and E. G. Njoku (2004), Soil moisture retrieval using the passive/active L- and S-band radar/radiometer, *IEEE Trans. Geosci. Remote Sens.*, *41*(12), 2792–2801.

Bowen, I. S. (1926), The ratio of heat losses by conduction and by evaporation from any water surface, *Phys. Rev.*, *27*, 779–787.

Brutsaert, W. A. (1982), *Evaporation Into the Atmosphere*, 299 pp., D. Reidel, Dordrecht, Netherlands.

Cai, X., Z.-L. Yang, C. H. David, G.-Y. Niu, and M. Rodell (2014), Hydrological evaluation of the Noah-MP land surface model for the Mississippi River Basin, *J. Geophys. Res. Atmos.*, *119*, 23–38, doi:10.1002/2013JD020792.

Carminati, A., and D. Vetterlein (2013), Plasticity of rhizosphere hydraulic properties as a key for efficient utilization of scarce resources, *Ann. Bot-London*, *112*(2), 277–290, doi:10.1093/Aob/Mcs262.

Carminati, A., A. B. Moradi, D. Vetterlein, P. Vontobel, E. Lehmann, U. Weller, H. J. Vogel, and S. E. Oswald (2010), Dynamics of soil water content in the rhizosphere, *Plant Soil*, *332*(1–2), 163–176, doi:10.1007/s11104-010-0283-8.

Carminati, A., C. L. Schneider, A. B. Moradi, M. Zarebanadkouki, D. Vetterlein, H. J. Vogel, A. Hildebrandt, U. Weller, L. Schuler, and S. E. Oswald (2011), How the rhizosphere may favor water availability to roots, *Vadose Zone J.*, *10*(3), 988–998, doi:10.2136/Vzj2010.0113.

Chang, H., A. Kumar, D. Niyogi, U. C. Mohanty, F. Chen, and J. Dudhia (2009), The role of land surface processes on the mesoscale simulation of the July 26, 2005 heavy rain event over Mumbai, India, *Global Planet. Change*, *67*, 87–103, doi:10.1016/j.gloplacha.2008.12.005.

Chen, F., and J. Dudhia (2001), Coupling an advanced land surface-hydrology model with the Penn State-NCAR MM5 modeling system. Part I: Model implementation and sensitivity, *Mon. Weather Rev.*, *129*(4), 569–585, doi:10.1175/1520-0493(2001)129<0569:Caalsh>2.0.Co;2.

Chen, F., and K. Mitchell (1999), Using GEWEX/ISLSCP forcing data to simulate global soil moisture fields and hydrological cycle for 1987–1988, *J. Meteorol. Soc. Jpn.*, *77*, 1–16.

Chen, F., and Y. Zhang (2009), On the coupling strength between the land surface and the atmosphere: From viewpoint of surface exchange coefficients, *Geophys. Res. Lett.*, *36*, L10404, doi:10.1029/2009GL037980.

Chen, F., K. Mitchell, J. Schaake, Y. Xue, H. Pan, V. Koren, Y. Duan, M. Ek, and A. Betts (1996), Modeling of land-surface evaporation by four schemes and comparison with FIFE observations, *J. Geophys. Res.*, *101*, 7251–7268, doi:10.1029/95JD02165.

Chen, F., Z. Janjic, and K. Mitchell (1997), Impact of atmospheric surface layer parameterization in the new land-surface scheme of the NCEP mesoscale Eta numerical model, *Boundary Layer Meteorol.*, *85*, 391–421.

Chen, F., T. Warner, and K. Manning (2001), Sensitivity of orographic moist convection to landscape variability: A study of the Buffalo Creek, Colorado, flash-flood case of 1996, *J. Atmos. Sci.*, *58*, 3204–3223.

Chen, F., et al. (2007), Description and evaluation of the characteristics of the NCAR High-Resolution Land Data Assimilation System during IHOP-02, *J. Appl. Meteorol. Climatol.*, *46*, 694–713.

Chen, F., et al. (2014), Modeling seasonal snowpack evolution in the complex terrain and forested Colorado Headwaters region: A model inter-comparison study, *J. Geophys. Res. Atmos.*, *119*, 13,795–13,819, doi:10.1002/2014JD022167.

Chen, Y. Y., K. Yang, W. J. Tang, J. Qin, and L. Zhao (2012), Parameterizing soil organic carbon's impacts on soil porosity and thermal parameters for eastern Tibet grasslands, *Sci. China Earth Sci.*, *55*(6), 1001–1011, doi:10.1007/s11430-012-4433-0.

Chenu, C. (1993), Clay polysaccharide or sand polysaccharide associations as models for the interface between microorganisms and soil: Water related properties and microstructure, *Geoderma*, *56*(1–4), 143–156, doi:10.1016/0016-7061(93)90106-U.

Cosby, B. J., G. M. Hornberger, R. B. Clapp, and T. R. Ginn (1984), A statistical exploration of the relationships of soil-moisture characteristics to the physical properties of soils, *Water Resour. Res.*, *20*, 682–690, doi:10.1029/WR020i006p00682.

Cosgrove, B. A., et al. 2003: Land surface model spin-up behavior in the North American Land Data Assimilation System (NLDAS). *J. Geophys. Res.*, *108*(D22), 8845, doi:10.1029/2002JD003316.

Dai, Y. J., et al. (2003), The common land model, *Bull. Am. Meteorol. Soc.*, *84*(8), 1013–1023, doi:10.1175/Bams-84-8-1013.

Darrah, P. R. (1993), The rhizosphere and plant nutrition: A quantitative approach, *Plant Soil*, *155*, 1–20, doi:10.1007/BF00024980.

Dickinson, R. E., Henderson-Sellers A., and P. J. Kennedy (1986), Biosphere/Atmosphere Transfer Scheme (BATS) for the NCAR Community Climate Model, National Center for Atmospheric Research, *NCAR Tech. Note NCAR/TN-275+STR*.

Gao, Y., S. Lu, and G. Cheng (2004), Simulation of rainfall and watershed convergence process in upper reaches of Heihe River Basin, July 2002, *Sci. China Ser. D Earth Sci.*, *47*, 1–8.

Gao, Y., et al. (2008), Enhancement of land surface information and its impact on atmospheric modeling in the Heihe River Basin, northwest China, *J. Geophys. Res.*, *113*, D20S90, doi:10.1029/2008JD010359.

Gregory, P. J. (2006), Roots, rhizosphere and soil: The route to a better understanding of soil science?, *Eur. J. Soil Sci.*, *57*(1), 2–12, doi:10.1111/j.1365-2389.2005.00778.x.

Hinsinger, P., G. R. Gobran, P. J. Gregory, and W. W. Wenzel (2005), Rhizosphere geometry and heterogeneity arising from root-mediated physical and chemical processes, *New Phytol.*, *168*(2), 293–303, doi:10.1111/j.1469-8137.2005.01512.x.

Hinsinger, P., A. G. Bengough, D. Vetterlein, and I. M. Young (2009), Rhizosphere: Biophysics, biogeochemistry and ecological relevance, *Plant Soil*, *321*(1–2), 117–152, doi:10.1007/s11104-008-9885-9.

Huang, C., X. Zheng, A. Tait, Y. Dai, Z. Chen, T. Li, and Z. Wang (2013), On using smoothing spline and residual correction to fuse rain gauge observations and remote sensing data, *J. Hydrol.*, *508*, 410–417.
Jordan, R. (1991), A one-dimensional temperature model for a snow cover, *Spec. Rep.* 91–16, Cold Reg. Res. and Eng. Lab., U.S. Army Corps of Eng., Hanover, N. H.
Koren, V., J. C. Schaake, K. E. Mitchell, Q.-Y. Duan, F. Chen, and J. M. Baker (1999), A parameterization of snowpack and frozen ground intended for NCEP weather and climate models, *J. Geophys. Res.*, *104*, 19,569–19,585, doi:10.1029/1999JD900232.
Koster, R., and C. P. Milly (1997), The interplay between transpiration and runoff formulations in land surface schemes used with atmospheric models, *J. Clim.*, *10*, 1578–1591.
Kumar, A., F. Chen, M. Barlage, M. Ek, and D. Niyogi (2014), Assessing impacts of integrating MODIS vegetation data in the Weather Research and Forecasting (WRF) model coupled to two different canopy-resistance approaches, *J. Appl. Meteorol. Climatol.*, *53*, 1362–1380, doi:10.1175/JAMC-D-13-0247.1.
Lakshmi, V. (2004), The role of satellite remote sensing in the prediction of ungauged basins, *Hydrol. Processes*, *18*(5), 1029–1034.
Lawrence, D. M., and A. G. Slater (2008), Incorporating organic soil into a global climate model, *J. Clim. Dyn.*, *30*, 145–160.
LeMone, M., M. Tewari, F. Chen, and J. Dudhia (2013), Objectively determined fair-weather convective boundary layer depths in the ARW-WRF NWP model and their comparison to CASES-97 observations, *Mon. Weather Rev.*, *141*, 30–54, doi:10.1175/MWR-D-12-00106.1.
LeMone, M., M. Tewari, F. Chen, and J. Dudhia (2014), Objectively-determined fair-weather NBL features in the ARW-WRF model and their comparison to CASES-97 observations, *Mon. Weather Rev.*, *142*, 2709–2732, doi:10.1175/MWR-D-13-00358.1.
Lewis, J. M. (1995), The story behind the Bowen ratio, *Bull. Am. Meteorol. Soc.*, *76*, 2433–2443.
Li, K., Y. Gao, F. Chen, J. Xu, Y. Jiang, L. Xiao, R. Li, and Y. Pan (2015), Simulation of the impact of roots on the soil moisture and surface fluxes in the central Tibetan Plateau, *Plateau Meteorol.*, *34*(3), 642–652.
Li, T., et al. (2014), Mapping near-surface air temperature, pressure, relative humisity and wind speed over Mainland China with high spatio-temporal resolution, *Adv. Atmos. Sci.*, *31*(5), 1127–1135.
Matsui, T., V. Lakshmi, and E. Small (2005), The effects of satellite-derived vegetation cover variability on simulated land–atmosphere interactions in the NAMS, *J. Clim.*, *18*(1), 21–40.
McCully, M. E., and J. S. Boyer (1997), The expansion of maize root-cap mucilage during hydration. 3. Changes in water potential and water content, *Phys. Plant.*, *99*(1), 169–177, doi:10.1034/j.1399-3054.1997.990123.x.
Moradi, A. B., A. Carminati, D. Vetterlein, P. Vontobel, E. Lehmann, U. Weller, J. W. Hopmans, H. J. Vogel, and S. E. Oswald (2011), Three-dimensional visualization and quantification of water content in the rhizosphere, *New Phytol.*, *192*(3), 653–663, doi:10.1111/j.1469-8137.2011.03826.x.
Nakanishi, T. M., Y. Okuni, Y. Hayashi, and H. Nishiyama (2005), Water gradient profiles at bean plant roots determined by neutron beam analysis, *J. Radioanal. Nucl. Chem.*, *264*(2), 313–317, doi:10.1007/s10967-005-0713-x.
Niu, G.-Y., and Z.-L. Yang (2006), Effects of frozen soil on snowmelt runoff and soil water storage at a continental scale, *J. Hydrometeorol.*, *7*, 937–952, doi:10.1175/JHM538.1.
Niu, G.-Y., Z.-L. Yang, R. E. Dickinson, and L. E. Gulden (2005), A simple TOPMODEL-based runoff parameterization (SIMTOP) for use in global climate models, *J. Geophys. Res.*, *110*, D21106, doi:10.1029/2005JD006111.
Niu, G.-Y., et al. (2011), The community Noah land surface model with multiparameterization options (Noah-MP): 1. Model description and evaluation with local-scale measurements, *J. Geophys. Res.*, *116*, D12109, doi:10.1029/2010JD015139.
Or, D., S. Phutane, and A. Dechesne (2007), Extracellular polymeric substances affecting pore-scale hydrologic conditions for bacterial activity in unsaturated soils, *Vadose Zone J.*, *6*(2), 298–305, doi:10.2136/Vzj2006.0080.
Peters-Lidard, C. D., E. Blackburn, X. Liang, and E. F. Wood (1998), The effect of soil thermal conductivity parameterization on surface energy fluxes and temperatures, *J. Atmos. Sci.*, *55*, 1209–1224.
Rasmussen, R., et al. (2011), High-resolution coupled climate runoff simulations of seasonal snowfall over Colorado: A process study of current and warmer climate, *J. Clim.*, *24*, 3015–3048.
Read, D. B., P. J. Gregory, and A. E. Bell (1999), Physical properties of axenic maize root mucilage, *Plant Soil*, *211*(1), 87–91, doi:10.1023/A:1004403812307.
Reeder S., M. Zarebanadkouki, E. Kroener, M. Ahmed, A. Carminati, and S. Kostka(2014), Rewetting rate of dry rhizosphere limited by mucilage viscosity and mucilage hydrophobicity, #H31D-0650 presented at 2014 Fall Meeting AGU.
Roberson, E. B., and M. K. Firestone (1992), Relationship between desiccation and exopolysaccharide production in a soil pseudomonas sp., *Appl. Environ. Microb.*, *58*(4), 1284–1291.
Sellers, P. J., D. A. Randall, G. J. Collatz, J. A. Berry, C. B. Field, D. A. Dazlich, C. Zhang, G. D. Collelo, and L. Bounoua (1996), A revised land surface parameterization (SiB2) for atmospheric GCMs.1. Model formulation, *J. Clim.*, *9*(4), 676–705, doi:10.1175/1520-0442.
Sheffield, J., G. Goteti, and E. F. Wood (2006), Development of a 50-yr high-resolution global dataset of meteorological forcings for land surface modeling, *J. Clim.*, *19*(13), 3088–3111.
Su, Z., T. Zhang, Y. Ma, L. Jia, and J. Wen (2006), Energy and water cycle over the Tibetan Plateau: Surface energy balance and turbulent heat fluxes, *Adv. Earth Sci.*, *21*, 1224–1236.
Tanaka, K., I. Tamagawa, H. Ishikawa, Y.-M. Ma, and Z. Hu (2003), Surface energy and closure of the eastern Tibetan Plateau during the GAME-Tibet IOP 1998, *J. Hydrol.*, *283*, 169–183.
Trier, S. B., F. Chen, and K. W. Manning (2004), A study of convection initiation in a mesoscale model using high-resolution land surface initial conditions, *Mon. Weather Rev.*, *132*, 2954–2976, doi:10.1175/MWR2839.1.
Trier, S. B., M. A. LeMone, F. Chen, and K. W. Manning (2011), Effects of surface heat and moisture exchange on ARW-WRF/Noah model 0-24-h warm-season precipitation forecasts over the central United States, *Weather Forecasting*, *26*, 3–25.
Trier, S., F. Chen, K. Manning, M. A. LeMone, and C. Davis (2008), Sensitivity of the simulated PBL and precipitation to land surface conditions for a 12-day warm-season convection period in the Central United States, *Mon. Weather Rev.*, *136*, 2321–2343.
Verseghy, D. L. (1991), CLASS-A Canadian land surface scheme for GCMS: I. Soil model, *Int. J. Climatol.*, *11*, 111–133, doi:10.1002/joc.3370110202.
Watt, M., M. E. Mccully, and M. J. Canny (1994), Formation and stabilization of rhizosheaths of Zea-Mays L: Effect of soil-water content, *Plant Physiol.*, *106*(1), 179–186.
Xu, X., C. Lu, X. Shi, and Y. Ding (2010), The large-scale topography of China: A factor for seasonal march of the Meiyu-Baiu-Changma in East Asia, *J. Geophys. Res.*, *115*, D02110, doi:10.1029/2009JD012444.
Xue, Y., R. Vasic, Z. Janjic, Y. M. Liu, and P. C. Chu (2012), The impact of spring subsurface soil temperature anomaly in the western U.S. on North American summer precipitation: A case study using regional climate model downscaling, *J. Geophys. Res.*, *117*, D11103, doi:10.1029/2012JD017692.

Yanai, M., and G. Wu (2006), Effects of the Tibetan Plateau, in *The Asian Monsoon*, *Praxis*, edited by B. Wang, pp. 513–549, Springer, New York.
Yanai, M. H., C. F. Li, and Z. S. Song (1992), Seasonal heating of the Tibetan Plateau and its effects on the evolution of the Asian summer monsoon, *J. Meteorol. Soc. Jpn.*, *70*(1B), 319–351.
Yang, K., T. Koike, H. Ishikawa, and Y.-M. Ma (2004), Analysis of the surface energy budget at a site of GAME/Tibet using a single-source model, *J. Meteorol. Soc. Jpn.*, *82*, 131–153.
Yang, K., T. Koike, B. S. Ye, and L. Bastidas (2005), Inverse analysis of the role of soil vertical heterogeneity in controlling surface soil state and energy partition, *J. Geophys. Res.*, *110*, D08101, doi:10.1029/2004JD005500.
Yang, K., T. Koike, H. Ishikawa, J. Kim, X. Li, H. Liu, S. Liu, Y. Ma, and J. Wang (2008), Turbulent flux transfer over bare-soil surfaces: Characteristics and parameterization, *J. Appl. Meteorol. Climatol.*, *40*(1), 276–290, doi:10.1175/2007JAMC1547.1.
Yang, K., Y. Y. Chen, and J. Qin (2009), Some practical notes on the land surface modeling in the Tibetan Plateau, *Hydrol Earth Syst Sci*, *13*(5), 687–701.
Yang, K., J. He, W. Tang, J. Qin, and C. Cheng (2010), On downward shortwave and longwave radiations over high altitude regions: Observation and modeling in the Tibetan Plateau, *Agric. For. Meteorol.*, *150*(1), 38–46, doi:10.1016/j.agrformet.2009.08.004.
Yang, Z.-L., G.-Y. Niu, K. E. Mitchell, F. Chen, M. B. Ek, M. Barlage, K. Manning, D. Niyogi, M. Tewari, and Y. Xia (2011), The community noah land surface model with multi-parameterization options (Noah-MP): 2. Evaluation over global river basins, *J. Geophys. Res.*, D12110, doi:10.1029/2010JD015140.
Yeh, T.-C., and Y.-X. Gao (1979), *The Meteorology of the Qinghai-Xizang (Tibet) Plateau* [in Chinese], 278 pp., Science Press, Beijing.
Yen T. F. (2001), In-situ stabilization of subsurface contaminants using microbial polymers. In Proc. of Industry Partnerships for Environmental Science Technology Conf., Morgantown, WV. 30 Oct.–1 Nov. USDOE-NETL, Morgantown, WV.
Young, I. M. (1995), Variation in moisture contents between bulk soil and the rhizosheath of wheat (Triticum-Aestivum L Cv Wembley), *New Phytol.*, *130*(1), 135–139, doi:10.1111/j.1469-8137.1995.tb01823.x.
Zhang, G., G. Zhou, F. Chen, and Y. Wang (2014a), Analysis of the variability of canopy resistance over a desert steppe site in inner Mongolia, China, *Adv. Atmos. Sci.*, doi:10.1007/s00376-013-3071-6.
Zhang, G., G. Zhou, F. Chen, M. Barlage, and L. Xue (2014b), A trial to improve surface heat exchange simulation through sensitivity experiments over a desert steppe site, *J. Hydrometeorol.*, *15*, 664–684, doi:10.1175/JHM-D-13-0113.1.
Zhang, S., X. Li, Y. Ma, G. Zhao, L. Li, J. Chen, Z. Jiang, and Y. Huang (2014c), Interannual and seasonal variability in evapotranspiration and energy partitioning over the alpine riparian shrub Myricaria Squamosa Desv. on Qinghai–Tibet Plateau, *Cold Reg. Sci. Technol.*, *102*(6), 8–20.